The run-on oligomer filament enzyme mechanism of SgrAI. Part 2: Kinetic modeling of the full DNA cleavage pathway

Chad K. Park, Jonathan L. Sanchez, Claudia Barahona, L. Emilia Basantes, Juan Sanchez, Christian Hernandez, and N. C. Horton

From the Department of Molecular and Cellular Biology, University of Arizona, Tucson, AZ 85721

Running title: *Run-on oligomerization and enzyme regulation*

To whom correspondence should be addressed: N.C. Horton, phone: (520) 626-3828, email: nhorton@email.arizona.edu

Keywords: DNA endonuclease, enzyme kinetics, enzyme mechanism, protein self-assembly, allosteric regulation

ABSTRACT

Filament or run-on oligomer formation by enzymes is now recognized as a widespread phenomenon with potentially unique enzyme regulatory properties and biological roles. SgrAI is an allosteric type II restriction endonuclease that forms run-on oligomeric filaments with activated DNA cleavage activity and altered DNA sequence specificity. In this two-part work, we measure individual steps in the run-on oligomer filament mechanism to address specific questions of cooperativity, trapping, filament growth mechanisms, and sequestration of activity using fluorophore labeled DNA, kinetic FRET measurements, and reaction modeling with global data fitting. The final models and rate constants show that the assembly step involving association of SgrAI/DNA complexes into the run-on oligomer filament is relatively slow (three to four orders of magnitude slower than diffusion limited) and rate limiting at low to moderate concentrations of SgrAI/DNA. The disassembly step involving dissociation of complexes of SgrAI/DNA from each other in the run-on oligomer filament is the next slowest step, but is fast enough to limit the residence time of any one copy of SgrAI or DNA within the dynamic filament. Further, the rate constant for DNA cleavage is found to be four orders of magnitude faster in the run-on oligomer filament than in isolated SgrAI/DNA complexes, and faster than dissociation of SgrAI/DNA complexes from the run-on oligomer filament, making the reaction efficient in that each association into the filament likely leads to DNA cleavage before filament dissociation.

Enzyme regulation via filament formation has only relatively recently been appreciated as a widespread phenomenon, and is implicated in the regulation of metabolism, signaling, and translation (1-7). This mechanism appears to have evolved independently in multiple systems, and may provide advantages such as rapid activation, storage of inactive enzymes, and buffering or sequestering of enzyme activity (2,6,8). Dysfunction in the control of such pathways is implicated in human diseases including cancer, diabetes, and developmental problems (2). Being a new enzyme mechanism, several important questions regarding the mechanism remain unknown and are addressed in this two-part work using the SgrAI system.

SgrAI is an allosteric, type II restriction endonuclease (RE) which in its activated state forms a filamentous structure we call a run-on oligomer (ROO[1]). SgrAI derives from the bacterium

[1]Abbreviations used are: 18M-1, 18 bp DNA containing the primary SgrAI recognition sequence, bp, base pair or

Streptomyces griseus, and is part of bacterial immunity against bacterial viruses (*i.e.* bacteriophage). Bacteria and their corresponding phage are among the oldest and most numerous organisms on Earth, evolving and co-evolving strategies of attack and defense in what is known as the "phage-host arms race" (9). In this "arms race", properties such as speed likely matter, such that SgrAI is able to cleave the invading phage DNA prior to viral transcription or replication. At the same time, damaging double stranded DNA cleavage of the host genome must be minimized and therefore the potentially destructive activity of SgrAI must be sequestered to the phage DNA.

The unusual mechanism evolved by SgrAI involving ROO filament formation may be a result of the particular biological niche found in *Streptomyces griseus*. SgrAI cleaves two types of recognition sites, primary (CRCCGGYG, 3 unique sequences) and secondary (CRCCGGY(A or C or T) and CRCCGGGG, 14 unique sequences), but will cleave the secondary sites only when on the same DNA as a primary site, or alternatively *in cis* when concentrations of SgrAI bound to primary site DNA are high (10,11). Primary sites are protected from DNA cleavage by the cognate SgrAI methyltransferase in the host organism. However, invading phage DNA will not be methylated at the primary site sequences, and hence SgrAI enzymes will bind to those sites, assemble into ROO filaments and rapidly cleave the DNA. The ROO filament will also incorporate SgrAI bound to secondary sites within the phage DNA, activating SgrAI and resulting in rapid cleavage of those sequences as well. This expansion of specificity to include secondary site sequences may have evolved to increase the number of cleavage sites in invading phage DNA, since the primary recognition site is relatively long (8 bp vs. 4-6 bp of many REs). The longer recognition site may have evolved to protect the host genome, which is also relatively large. More host DNA means more recognition sites which must be protected by the cognate methyltransferase or be cleaved by SgrAI. This may also explain the unusually slow cleavage rate of SgrAI in the absence of ROO filament formation (rate constant of 0.1 min^{-1}, compared to 20 min^{-1} of the RE EcoRI (12)). However, the slow DNA cleavage rate and rare recognition sequence makes for very poor anti-phage activity. But the allosteric activation by binding and ROO filament assembly with multiple unmethylated primary sites increases the DNA cleavage rate by 200-1000 fold (8,13). In addition, the expansion of DNA sequence specificity from 3 primary sites to also include the 14 secondary site sequences results in very rapid cleavage of many sites on the phage DNA, making for an effective anti-phage enzyme.

Structural studies of SgrAI in its low activity form show a canonical dimeric RE fold enzyme bound to one recognition site (primary or secondary) in duplex DNA (14,15). These SgrAI/DNA complexes are then the building blocks for the high activity state of SgrAI which forms a left-handed helix with approximately four SgrAI/DNA complexes per turn which we call a run-on oligomer or ROO filament (**Fig. 1A**)(16). The SgrAI/DNA complexes associate using protein-protein and protein-DNA interactions between neighboring SgrAI/DNA complexes (**Fig. 1A**), and the DNA (when contiguous sites are bound by SgrAI) is predicted to weave in and out of the filament (17). The ROO filament can also theoretically extended indefinitely from either end, and ROO filaments of 30 or more SgrAI/DNA complexes have been visualized via electron microscopy (16). The conformation of SgrAI is altered in the ROO filamentous activated state compared to the un-oligomerized low activity state, as expected for an allosteric enzyme (16).

Since SgrAI bound to primary site DNA forms the ROO filament, which also binds and activates SgrAI bound to secondary site DNA, the primary site DNA is an allosteric effector of both the activity and substrate specificity of SgrAI. To explain this allosteric behavior, a model has been proposed wherein SgrAI exists in equilibrium between an active and an inactive conformation (16). The active

base pairs, ES_{DNA}, SgrAI bound to uncleaved DNA containing a primary SgrAI recognition sequence, ES_{18}, SgrAI bound to uncleaved 18M-1, EP_{DNA}, SgrAI bound to cleaved DNA, EP_{40}, SgrAI bound to self-annealed PC DNA, EP_{18}, SgrAI bound to 18M-1 cleaved in the SgrAI pattern, Flo, 6-Carboxyfluorescein, Kintek GKE, Kintek Global Kinetic Explorer software, mw, molecular weight, nt, nucleotide or nucleotides, OAc, acetate, PC or PC DNA, pre-cleaved primary site DNA with 16 flanking bp DNA, ROO, run-on oligomer(s) formed from SgrAI bound to DNA, RE, restrictin endonuclease, Rox, Rhodamine-X or 5(6)-Carboxy-X-rhodamine.

conformation readily forms the ROO filament, and in turn, the ROO filament stabilizes the active conformation. The active conformation forms more readily (is more energetically stable) when SgrAI is bound to primary site than when bound to secondary site sequences, explaining why SgrAI bound to primary site DNA readily assemble into the ROO filaments, but SgrAI bound to secondary site DNA alone will not. The activated conformation has rapid DNA cleavage activity, thus DNA is rapidly cleaved by SgrAI in the ROO filament. ROO filaments assemble from SgrAI/DNA complexes, regardless of the state of cleavage of the DNA, hence the product of primary site DNA cleavage by SgrAI also stimulates SgrAI activity by inducing ROO filament formation. The formation of ROO filaments intuitively suggests cooperativity and rapid activation, however until this study, the details of these effects were not known or quantified. In addition, the ROO filament structure suggests potential trapping of cleaved DNA, yet the rapid turnover in steady state reactions indicates that trapping does not occur (11).

In this two-part work, we measure individual steps in the run-on oligomer mechanism to address specific questions of cooperativity, trapping, filament growth mechanisms, and sequestration of activity using fluorophore labeled DNA, kinetic FRET measurements, and reaction modeling with global data fitting. The first part (Part 1 (18)) developed reaction models for ROO filament formation and determined initial estimates of rate constants for assembly and disassembly of SgrAI/DNA complexes from the ROO filament. In this second to the two parts, we develop models further and globally fit all steps of the reaction pathway including DNA cleavage and product release. The reaction data were collected using four different experimental approaches. Each approach measures a different set of steps in the reaction pathway, and concentrations of activating and reporter DNA were varied in each timed reaction to provide additional information. The resulting data from a total of 22 different timed reactions were then fit globally to different reaction models of increasing complexity and ROO filament growth mechanisms, resulting in estimates of microscopic rate constants for each major step of the reaction pathway.

The resulting globally fit rate constants show several consistent trends across all models and mechanisms. First, the association of SgrAI/DNA complexes into the ROO filament is relatively slow and is three to four orders of magnitude slower than diffusion limited. We show that this characteristic is likely that which provides the sequestering effect necessary to prevent cleavage of secondary sites in the host DNA upon activation of SgrAI via invading phage. Secondly, the corresponding dissociation of SgrAI/DNA complexes from the ROO filament is the next slowest step, and this rate constant is the same to the best of our estimation regardless of whether the bound DNA is cleaved or not. Yet though it is the second slowest step of the overall reaction, this step is still fast enough to result in the rapid equilibration of individual SgrAI/DNA complexes into and out of the ROO filament. Therefore, trapping of SgrAI enzyme and/or product (cleaved) DNA within the ROO filament does not occur. Third, the DNA cleavage rate is four orders of magnitude faster in the ROO filament than in isolated SgrAI/DNA complexes, and is now comparable to those of other REs. Significantly, it is at least three times faster than the dissociation of SgrAI/DNA complexes from the ROO filament, hence cleavage of the DNA is likely upon every association of a SgrAI/DNA complex into the ROO filament, making the reaction mechanism efficient. The last step, product release (dissociation of the cleaved DNA from SgrAI) is fast and does not limit the overall DNA cleavage reaction. Finally, we use the different reaction models and extracted rate constants to address issues of cooperativity and growth mechanisms of the ROO filament.

RESULTS

Overview of methodology

Activated DNA cleavage by SgrAI involves several steps: 1) DNA binding by SgrAI, 2) assembly of SgrAI/DNA complexes into the filamentous assembly we call ROO filaments, 3) rapid DNA cleavage by SgrAI while in the ROO filament, 4) separation of the individual SgrAI/DNA complexes from the ROO filament, then 5) dissociation of the cleaved DNA from SgrAI. In addition, SgrAI will cleave primary site DNA sequences when un-oligomerized (*i.e.* not in the ROO filament), albeit at a slow rate (8). Also, the primary site DNA used to induce ROO filament formation and activate SgrAI (*i.e.* PC DNA in this work) is a mimic of the cleaved product DNA which must self-anneal before binding to SgrAI, and this annealing can limit the reaction rates at lower

concentrations of PC DNA.

Since the goal of this work is to estimate each individual, microscopic rate constant (forward and reverse) for each step, reaction data were measured using three different approaches. In addition, the number of rate constants to be fit was reduced by estimating equilibrium dissociation constants (K_D), and fixing reverse rate constants to the fitted forward rate constant. This was done for the self-annealing of PC DNA (K_D estimated in (18)) and for binding of DNA to SgrAI. The K_D of SgrAI for the DNA used in these studies was determined as described in the Supporting Information,

The association of SgrAI/DNA complexes into (and out of) the ROO filament was measured by placing FRET donor and acceptor fluorophores on different DNA molecules, resulting in a FRET signal when SgrAI bound to donor-DNA assembles with SgrAI bound to acceptor-DNA into the ROO filament (**Fig. 2A)**. A titration was first performed to show that the FRET technique measures ROO filament assembly (described below). Timed reactions were then measured to provide the data to use in global fitting to reaction models and from which to determine rate constants for each step of the reaction (Data Sets 4 and 6, **Table S1**). First, to isolate only ROO filament formation (and breakdown), DNA cleavage was blocked by excluding the required Mg^{2+} cofactor from the reaction buffer (reactions of Data Set 4). This approach is similar to that used in Part 1 (18), namely the approach to equilibrium method, although herein we use also a new DNA construct which is a shorter version of the acceptor labeled reporter DNA (*i.e.* 18M-1, an 18 bp DNA with one uncleaved primary recognition site). The 18 bp reporter DNA is used instead of the 40 bp reporter DNA of Part 1 (18) because it will not significantly induce ROO filament formation by SgrAI. The 18 bp construct cannot induce ROO filament formation presumably due to the shortened flanking bp on either side of the 8 bp recognition site, since those flanking bp make contacts to neighboring SgrAI/DNA complexes in the ROO filament (see **Fig. 1A**) (8,13,16). Therefore, the activation of SgrAI can be controlled in reactions by using different concentrations of activator DNA (*i.e.* PC DNA, which self-associates into a 40 bp Pre-Cleaved DNA containing a single primary recognition site cleaved in the SgrAI pattern, and which was also used in Part 1 (18)). SgrAI bound to self-annealed PC DNA will induce ROO filament formation that can incorporate (and thereby activate) SgrAI bound to the 18 bp reporter DNA. In total, six different timed reactions, each having different concentrations of DNA (all with excess SgrAI), were measured and comprise Data Set 4 (**Table S1**).

Reaction mechanism models created to globally fit the reaction data of Data Set 4 are summarized in **Table 2** (the ***"Filament Assembly"*** mechanisms). It was not possible to build models allowing for infinitely long ROO filaments, though these are theoretically possible. Instead, the modeling software limited ROO filaments to only 4-5 SgrAI/DNA complexes total. However, this simplification is adequate for modeling the data since previous analyses done in Part 1 (18) showed that most ROO filaments are 4-5 SgrAI/DNA complexes in size or smaller when the total DNA concentration (corresponding to the total concentration of SgrAI recognition sites) is limited to 250 nM or lower, as is the case in these reactions (see **Table S1**).

Next, the growth mechanism of the ROO filaments was modeled to allow for either "ends only" or "breaks in the middle" mechanisms. The "ends only" mechanism limits ROO filament growth to only either end, and via the addition of only single SgrAI/DNA complexes at a time. In contrast, the "breaks in the middle" allows ROO filaments to grow via the association of two ROO filaments of any size (or single SgrAI/complexes as well), and to dissociate via "breakage" at anywhere within the ROO filament, between any adjacent SgrAI/DNA complex. The implications and justifications for these mechanisms are discussed below.

To gain more information on steps following ROO filament formation (including DNA cleavage and product release), we also used an approach where the reporter DNA is doubly labeled with both donor and acceptor (**Fig. 2B**). This allowed the FRET signal to be lost upon the dissociation of cleaved DNA from SgrAI (due to strand separation of short, unstable duplexes), hence measuring steps following DNA cleavage, ROO filament dissociation, and release of cleaved DNA. These reactions are collected into Data Set 5. We also used this DNA to gain kinetic information on reaction steps up to and including DNA cleavage, but not product release, by analyzing the total amount of cleaved DNA via denaturing PAGE. This approach was used in the timed reactions of Data Set 7. Data

Set 6 contains reaction data from the same approach as used in Data Set 4 reactions (activator and reporter DNAs are singly labeled with FRET donor and acceptor, respectively), however Mg^{2+} is included in the reactions, allowing for the full DNA cleavage pathway to be performed by SgrAI.

Modeling of the full DNA cleavage reaction data (Data Sets 5-7, with a total of 22 timed reactions) was performed separately from the approach to equilibrium data used with Data Set 4. Different reaction models were built based on those used in Data Set 4, however extended to include DNA cleavage, as well as subsequent steps. These models are also summarized in **Table 2** (*i.e.* ***"Full Pathway"*** models) and were tested for their ability to fit the experimental timed reaction data. Despite the differing degrees of complexity (maximum ROO filament length and filament growth mechanisms, independent or simultaneous DNA strand cleavage and cleavage with the ROO filament) fitting with these models resulted in very similar extracted microscopic rate constants and similar measures of the quality of fit (see **Tables 3-7, Fig. S5,** and below).

FRET titration showing ROO filament formation

FRET between donor (Flo, 6-Carboxyfluorescein) and acceptor (Rox, Rhodamine-X or 5(6)-Carboxy-X-rhodamine) labeled DNA (see Experimental Procedures and **Fig. S1)** was used to investigate the equilibrium association of SgrAI/DNA complexes into run-on oligomer (ROO) filaments. DNA cleavage by SgrAI was prevented from occurring by excluding the necessary Mg^{2+} cofactor from the reaction buffer, and instead using Ca^{2+} as a mimic, which inhibits DNA cleavage (8). A limiting concentration (50 nM) of acceptor labeled reporter DNA (Rox-18M-1) was mixed with 2-4 μM SgrAI and then titrated with increasing concentrations of DNA containing donor (fluorescein) labeled DNA (either Flo-18M-1 or Flo-PC). The fluorescence emission (using 498 nm excitation, the excitation maximum of Flo, the donor) was measured at 508-700 nm before and after each addition in this titration. The emission contained emitted light from both donor Flo ($\lambda^{emission}$(max)=520 nm) and acceptor Rox ($\lambda^{emission}$(max)=608 nm) fluorophores. To isolate the acceptor emission due to FRET, the contributions from donor emission, as well as that which occurs from the acceptor in the absence of donor, were subtracted (see Experimental Procedures).

The resulting emission spectra increased with increasing concentrations of total Flo-PC DNA (**Fig. 3A**). In **Figure 3** we show emissions as a function of total [EP_{40}] (for Enzyme Product of 40 bp, which is SgrAI bound to self-annealed Flo-PC DNA, see **Fig. 2A**), rather than Flo-PC DNA concentration, to allow comparison with the other titrations (**Table 1)**. This is reasonable since SgrAI binds to self-annealed PC DNA with a K_D in the low nM range (18), and [SgrAI] is in the μM range in the titrations so nearly all PC DNA should be bound by SgrAI. The increase in FRET observed in **Fig. 3A** is plotted vs. total [EP_{40}] in **Fig. 3B** (red) and fit to the Hill equation giving $K_{1/2}$ (*i.e.* [EP_{40}] giving the half maximum FRET signal) of 0.50±0.02 μM. The Hill coefficient for the fit, a measure of cooperativity on total [EP_{40}], was found to be 2.5. This data is summarized in **Table 1**. For comparison, no such increase in in FRET is seen when SgrAI is absent (black, **Fig. 3B**).

A second titration was performed to test the assumption that SgrAI bound to the shorter DNA (18M-1) would not significant induce ROO filament formation (8). In this case, instead of Flo-PC DNA, Flo-18M-1 was titrated into the reaction with Rox-18M-1 and excess SgrAI, and FRET measured. **Figure S2A** shows the result. Little FRET is found until very high concentrations of Flo-18M-1 (and consequently Flo-ES_{18}, for Enzyme Substrate of 18 bp, SgrAI bound to Flo-18M-1). The Hill plot in **Figure S2B** shows a curve that has not reached saturation even at at 3.5 μM ES_{18}. This result is also summarized in **Table 1**, along with the similar titration performed in Part 1 (18) with Rox-40-1 (a 40 bp DNA with a single primary site) and Flo-PC.

Although the $K_{1/2}$ determined by these FRET titrations are not equilibrium dissociation constants, (K_D), since ROO filament formation is more complex than simple 1:1 binding, they reflect the affinities of SgrAI/DNA complexes to each other within the ROO filament. The data of **Table 1** indicates that the ROO filament forms more readily (requiring lower concentrations) when the DNA contains longer flanking regions, as in case of the longer DNA constructs PC DNA and 40-1 (each having 16 bp flanking the primary recognition sequence). In contrast, SgrAI bound to 18M-1 (with just 5 flanking bp on either side of the primary recognition sequence) only weakly self-associates into the ROO filament (**Table 1**). However, the

assembly formed between SgrAI/DNA complexes where both DNAs have longer flanking regions (*i.e.* PC DNA and 40-1) has the lowest $K_{1/2}$ (0.16 μM, **Table 1**). When one DNA is shorter (18M-1) and one longer (PC DNA), the $K_{1/2}$ is intermediate (0.5 μM, **Table 1**). These results are consistent with the CryoEM structure of the run-on oligomer formed by SgrAI bound to PC DNA, showing contacts between the flanking DNA of one SgrAI/DNA complex to adjacent SgrAI/DNA complexes (**Fig. 1**). The shorter flanking DNA of 18M-1 cannot make these contacts, hence self-association of ES_{18} into the ROO filament is much weaker. This also explains why SgrAI activation is dependent on DNA length, and why 18M-1 is unable to provide activation (8,16). Similarly, results from mutagenesis of residues at this protein-DNA interface show the importance of these contacts between the flanking DNA and neighboring SgrAI/DNA complexes in the ROO filament. For example, mutations removing a positive charge or introducing a negative to this interface disrupt activated cleavage by SgrAI, also presumably by weakening the ROO filament (13).

Dissociation of ROO filament with DNA cleavage and the absence of DNA trapping

To investigate if trapping of SgrAI bound to product DNA occurs, the FRET titration discussed above with DNAs Rox-18M-1 and Flo-PC (but without Ca^{2+} present) was repeated, and then Mg^{2+} added to allow DNA cleavage by SgrAI. Upon cleavage and dissociation of Rox-18M-1 from SgrAI, the shortened DNA duplex is unstable and rapidly dissociates irreversibly to single strands, making the reaction irreversible. Spectra were taken before and after the addition of 10 mM $MgCl_2$. **Figure S3** shows that after 30 minutes very little FRET signal remains, indicating that very few complexes containing both SgrAI/Rox-18M-1 and SgrAI/Flo-PC remain. Thus, no significant trapping of Rox-18M-1 in ROO filaments occurs.

Timed approach to equilibrium reactions to measure ROO filament assembly (Data Set 4)

FRET was used to detect the association of SgrAI/Rox-18M-1 complexes (*i.e.* Rox-ES_{18}) with SgrAI bound to two copies of Flo-PC (Flo-EP_{40})(see **Fig. 2A**). **Table S1** provides information on the independent timed reactions of Data Set 4, and **Fig. 4** shows time traces of the data with their global fits (using model ***"Filament Assembly 4BM"***, see **Table 2** and above for descriptions of models). Models were created to simulate the reaction and predict concentrations of species at a given time after reaction initiation (given appropriate starting concentrations and rate constants).

Note that in all models (See **Tables S3-S5** for reaction equilibria modeled and equations used to simulate timed FRET data) it was assumed that the kinetics of assembly and disassembly of the ROO filament are independent of ROO filament size, for example, the addition of a single SgrAI/DNA complex to a ROO filament of size 3 (having 3 SgrAI/DNA complexes) has the same association and dissociation rate constants as it would when associating to a ROO filament of size 4. This essentially assumes interactions occur *only* between adjacent SgrAI/DNA complexes within the ROO filament, and that assembly is non-cooperative. This assumption is tested and discussed further below.

In addition to modeling the self-association of PC DNA and DNA binding by SgrAI, the associations of interest in this work are those that form the ROO filament: 1) association of Rox-ES_{18} (SgrAI bound to Rox labeled 18mer) and Flo-EP_{40} (SgrAI bound to self-annealed Flo-PC, mimicking a 40 bp cleaved DNA), which gives the FRET signal, and 2) self-association of Flo-EP_{40}, which does not give a FRET signal. ES_{18} does not self-associate significantly, as assessed by the FRET titration (**Fig. S2**), and hence is not modeled, nor are ROO filaments with two adjacent ES_{18} (**Tables S3-S5**). **Table 3** summarizes the resulting rate constants derived from fitting each of the four ***"Filament Assembly"*** models to the 6 different reactions measured in Data Set 4. A total of 7 independent rate constants, and 12 baseline or scaling constants (for relating simulated concentrations of species to FRET signals measured in the timed reactions) were fit in each model (**Table 4**). Also shown in **Table 4** is the χ^2/DoF, a measure of the quality of the fit with 1 being optimal, which was found to be between 2.1-2.7 for fitting of the four different models to the same data (Data Set 4). The fitted rate constants for the self-association and dissociation of EP_{40} with itself were found to be very similar to those reported previously for EP_{40} and ES_{40} (18): $1.3x10^6$-$3x10^6$ $M^{-1}s^{-1}$ for the forward rate constant (k_4), and 0.01-0.06 s^{-1} for the reverse (k_{-4})(**Table 3**). In the case of the association and dissociation of ES_{18} and EP_{40}, similar values were found, $1.5x10^6$-$2x10^6$ $M^{-1}s^{-1}$ for the association rate constant (k_5), and 0.02-0.08 s^{-1} for the dissociation

rate constant (k_{-5})(**Table 3**). The 0.95 χ^2 threshold error boundaries (see Experimental Procedures and Supporting Information for how this is estimated) are given in parentheses for each rate constant (**Table 3**). The values and boundaries overlap for each independent rate constant determined from the four different models, as is also true for the two types of associations ($EP_{40} + EP_{40}$ and $EP_{40} + ES_{18}$)(see also **Fig. S5A-D)**. Since all four models give similar quality of fit parameters (**Table 4**), it can be concluded that the data and these models cannot distinguish between the different types of ROO filament growth mechanisms (*i.e.* "breaks in the middle" vs. "ends only"), and that models that limit filament size to 4 vs. 5 SgrAI/DNA complexes per ROO filament give similar rate constants.

DNA cleavage pathway measured via FRET with singly labeled reporter (Rox-18M-1) and activator (Flo-PC) DNA (Data Set 6)

Data Set 6 (see **Fig. 2A** for a reaction schematic) is similar to Data Set 4, however 10 mM $MgCl_2$ is included in the reaction allowing DNA cleavage by SgrAI. Following initiation by the addition of Rox-18M-1, emission intensities were recorded at both 520 nm (Flo emission) and through the 590 cut-on filter (Flo and Rox emissions). The 520 nm recording was used to remove Flo emission contributions from the 590 cut-on filter data (following appropriate scaling, see Experimental Procedures). This corrected filter data (CF) was used in global data fitting along with reactions of Data Sets 5 and 7 described below. **Table S1** summarizes the different reactions of Data Set 5.

DNA cleavage pathway measured via FRET with doubly labeled reporter (Flo-18M-1-Rox) and unlabeled activator DNA (PC DNA) (Data Set 5)

Data Set 5 utilizes doubly labeled reporter DNA (Flo-18M-1-Rox), unlabeled PC DNA, and allows for DNA cleavage by SgrAI due to the presence of Mg^{2+} in the reaction buffer (see **Fig. S2B** for a reaction schematic). Once the reporter DNA is cleaved and dissociated from SgrAI, and the two strands of the DNA duplex dissociate into single strands, the FRET signal between the Flo and Rox fluorophores is lost (**Fig. S2B**). We expect the dissociation into single strands to be irreversible because the predicted T_m (melting temperature) of the two halves of the cleaved 18M-1 DNA are 9-11°C and reactions were performed at 25°C. We also tested this irreversibility in a number of ways. **Fig. 5A** shows a before and after emission (using excitation of Flo at 498 nm) from a reaction (with Flo-18M-1-Rox), showing loss of FRET following the reaction (increase in Flo emission at 520 and loss of Rox emission at 605 nm). If annealing of the cleaved Flo-18M-1-Rox occurred, no such loss would occur. Further, additional reactions were performed in the presence of excess unlabeled single stranded complimentary DNA, to prevent any reannealing of cleaved product DNA. No differences in the recorded data were found (*data not shown*). Finally, additional evidence of the irreversibility of dissociated cleaved 18M-1 is shown in **Fig. S3**, where complete loss of FRET between Rox-18M-1 and Flo-PC in assemblies with SgrAI was seen following the addition of 10 mM $MgCl_2$.

Timed FRET reactions were performed as described above for Data Set 6, however the DNA used was unlabeled PC DNA and doubly labeled 18M-1 (Flo-18M-1-Rox). Data were recorded following the addition of SgrAI to the premixed solution using excitation at 498 nm and emission at 520 nm, which followed the unquenching of Flo due to the loss of FRET between Flo and Rox as the substrate (Flo-18M-1-Rox) DNA was cleaved and strand-separated (**Fig. 2B**). All timed reaction data sets are summarized in **Table S1**, and an example of a measured reaction with an analytical fit is shown in **Fig. 5B**. **Figs. 5C-D** are Hill plots of the analytically derived rate constants vs. the concentration of total [EP_{40}]. These give $K_{1/2}$ of 0.2±0.1 μM when N (the Hill coefficient, a measure of cooperativity) is forced to 1 (**Fig. 5C**) and $K_{1/2}$ of 2 μM, when N is allowed to be fit, giving 0.4±1 (**Fig. 5D**). These results do not support the presence of positive cooperativity of DNA cleavage and release by SgrAI on total EP_{40} concentration. Global fitting of Data Set 5 is done together with Data Sets 6-7 and is described below.

DNA cleavage pathway measured via doubly labeled reporter (Flo-18M-1-Rox), unlabeled activator (PC) DNA, and denaturing-PAGE (Data Set 7)

This data set is similar to Data Set 5 (see **Fig. 2B** for reaction schematic) in using Flo-18M-1-Rox, varied concentrations of PC DNA, and excess SgrAI in the presence of 10 mM $MgCl_2$, however instead of FRET measurements, the total amount of cleaved DNA (whether bound to SgrAI or not) was measured

by quenching 5 µl aliquots of a 100 µl reaction and analyzing via denaturing PAGE and densitometry of Flo and Rox containing bands. The reactions were repeated with different concentrations of PC DNA, resulting in varied concentrations of SgrAI bound to PC DNA (*i.e.* total [EP_{40}]). **Table S1** summarizes the 9 reactions and the results of analytical fits to each, an example of which is shown in **Fig. 6A**. **Figure 6B** shows a Hill plot of the analytically fitted rate constants, giving a $K_{1/2}$ of 0.5 µM and a Hill coefficient N of 1.0±0.2. This indicates that half-maximal DNA cleavage occurs at approximately 0.5 µM total [EP_{40}], and that the rate constant for DNA cleavage by SgrAI under these conditions, while dependent on total [EP_{40}], does not appear to be cooperative on total [EP_{40}] (since the Hill coefficient is ~1). Data Set 7 data is fit together with that of Data Sets 5-6 in global fitting to five different reaction models (described below).

Global Fitting of DNA Cleavage Reaction Data (Data Sets 5-7)

Reaction data from Data Sets 5-7 described above were fit together (globally) using five different reaction mechanism models (***"Full Pathway"*** models of **Table 2,** equations given in **Tables S6-S14)**. **Figure 7** summarizes one of the simpler models (***"Full Pathway 2mers"***), which includes the reversible association of single stranded activator (PC) DNA (with rate constants k_1 and k_{-1}), the reversible binding of self-annealed PC DNA and substrate DNA (18M-1) by SgrAI (rate constants k_2, k_{-2}, k_3, and k_{-3}), and then the reversible association of SgrAI/DNA complexes (EP_{40} and ES_{18}) into larger assemblies (rate constants k_5, k_{-5}). Though self-assembly of EP_{40} does occur, it is not modeled in this particular reaction model, and also ROO filaments of ES_{18} and EP_{40} are limited to size 2 with no larger filaments modeled. Cleavage of substrate DNA (18M-1) is rapid and irreversible in the ROO filament (rate constant k_6). Complexes which now contain EP_{18} (P for product, *i.e.* the cleaved 18mer) dissociate into EP_{40} and EP_{18} (k_5 and k_{-5}, same rate constants as with uncleaved 18M-1 in ES_{18}), and the cleaved 18M-1 DNA dissociates irreversibly from SgrAI (rate constant k_7). Other models include more complexity; the five global models of the full DNA cleavage pathway (summarized in **Table 2**) differ in several attributes including size of ROO filament (2-4 SgrAI/DNA complexes total) and growth mechanism ("breaking in the middle", *i.e.* ***BM***, or "ends only", *i.e.* ***EO***) as described above, as well as whether or not self-association of EP_{40} is included in the model. The cleavage of each individual strand of DNA in the 18M-1 DNA duplex is modeled in ***"Full Pathway 2mers Independent Strand Cleavage"***, and model "***Full Pathway 2mers"*** is exactly the same with the exception that only one step is modeled for duplex DNA cleavage. Models ***"Full Pathway 3mers", "Full Pathway 4EO",*** and "***Full Pathway 4BM"*** all have this simplification as well, and in addition, differ in the independence of DNA cleavage by different ES_{18} in the same ROO filament (**Table 2**). Of course, DNA cleavage by each ES_{18} is expected to be independent, as cleavage of each strand is also, but simplifications are necessitated by limitations of the modeling software, and simulations show that only very few of the ROO filaments contain more than one copy of ES_{18} (**Fig. S7C**). Another assumption and simplification that is present in all models is that ES_{18} and EP_{18} behave the same with respect to association to EP_{40}, meaning that the state of cleavage of the bound 18M-1 DNA does not affect the affinity of the SgrAI/DNA complex to a SgrAI/DNA complex containing PC DNA. The similar association and dissociation rate constants found in Part 1 with ES_{40} + ES_{40} and ES_{40} + EP_{40} support this assumption (18). The similar resulting fits (described below) and extracted rate constants from all five models indicate that these simplifications have a minimal effect on data fitting.

Figure 8 shows individual plots (simulated and experimental data) for representative reactions from using Data Sets 5-7 and using model "***Full Pathway 4BM"***. **Tables 5-6** show the derived rate constants for each reaction step along with error boundaries (plotted in **Fig. S5)**, and the quality of fit parameters are given in **Table 7**. The average of fitted rate constants for the self-association of EP_{40} (*i.e.* k_4) for the three models having such an association step is $1.4x10^5$ M^{-1} s^{-1}, with a range of $1.2x10^5$ to $1.7x10^5$ M^{-1} s^{-1} (**Table 5**, **Fig. S5A**). These are approximately tenfold slower than those found in the fitting of Data Set 4 (**Table 3**, **Fig. S5A**), containing approach to equilibrium reaction data measured without Mg^{2+}. Previous work also showed that this association rate constant was tenfold slower in the presence of 10 mM Ca^{2+} relative to that measured without divalent cations (18), suggesting a divalent cation effect on the association rate constant of SgrAI/DNA complexes into the ROO filament. Error boundaries of the rate constant indicate a range from $8x10^3$-

$7x10^5$ $M^{-1}s^{-1}$ among the five models, and model ***"Full Pathway 4BM"***, the most sophisticated model, gives an error interval (at a 0.95 χ^2 threshold) of $6x10^4$-$3x10^5$ $M^{-1}s^{-1}$ (**Table 5**).

Dissociation rate constants (k_{-4}) of EP_{40} from other EP_{40} fit best to 0.03 s^{-1}, although the analysis also suggests these to have a range of $3x10^{-6}$-1.0 s^{-1} (**Table 5, Fig. S5B)**. An average of 0.03 s^{-1} for this rate constant was also found in the fitting of Data Set 4 (**Table 3**), but with tighter boundary limits of $9x10^{-4}$-0.15 s^{-1}. Thus, the presence of the divalent cation (Mg^{2+} in the current case, no divalent cation for Data Set 4) does not appear to affect this rate constant in the current analysis, consistent with that observed using ES_{40} and EP_{40} (18).

The association rate constant for ES_{18}+ EP_{40} (or EP_{18}+EP_{40} when 18M-1 is cleaved)(k_5,**Table 5, Fig. S5C**) was found to be $2x10^5$-$2.5x10^5$ $M^{-1}s^{-1}$ in the five models, similar to that found for EP_{40} + EP_{40} (k_4, **Table 5**). Error analysis indicates a fairly tight boundary of 2-$3x10^5$ $M^{-1}s^{-1}$ (**Fig. S5C**), likely because this rate constant limits the overall reaction rates measured in all three Data Sets 5-7 (in most reactions).

The dissociation rate constant found for ES_{18} from EP_{40} (or EP_{18} from EP_{40}) (*i.e.* k_{-5}) of 0.06 s^{-1} was on average faster than that of EP_{40} from EP_{40} (k_{-4}, 0.03 s^{-1}), with a range of 0.04-0.08 s^{-1} in the various models, and fairly constrained error boundary of 0.04-0.10 s^{-1} (**Table 5, Fig. S5D**). This step appears to limit the overall reaction rates of the DNA cleavage reactions at the higher concentrations of PC DNA (and total [EP_{40}]), when the association of ES_{18} and EP_{40} is no longer rate limiting. For comparison, the average rate constant for the same reaction from fitting the approach to equilibrium data (*i.e.* Data Set 4) to the four different models is 0.05 s^{-1}, very similar to that found here in the full DNA cleavage pathway (k_{-5}, **Table 3, Fig. S5D**), however the error boundaries are far less constrained by the models with the "breaks in the middle" mechanism (*i.e.* types "***4BM***" and "***5BM***") compared to the "ends only" (*i.e.* types ***"5EO"*** and ***"4EO"***)(**Table 3**, **Fig. S5D**).

The DNA cleavage rate constant (k_6) was fit to an average of 0.7 s^{-1} and ranged from 0.5-0.8 s^{-1} (**Table 6, Fig. S5E**). The error analysis for the simpler three models were more constrained than the two more sophisticated models, with error boundaries of 0.2-1.0 s^{-1} (**Table 5, Fig. S5E**). For the more complex models, the boundaries are much larger, but a closer look at the error calculation for this parameter reveals a peak at the best fit parameter (See **Fig. S6E** for that of ***"Full Pathway 4BM"***), with a sharp drop-off for lower values but a shallower drop-off for higher. The shallow drop-off at the higher end is due to the fact that only 2-3 data points constrain the upper limit of this rate constant. These derive from two reactions of Data Set 7 (Reaction IDs 408 and 409, **Table S1**) having the highest concentration of PC DNA (and total [EP_{40}]) where association into the ROO filament is no longer rate limiting. Data Set 7 data with lower concentrations of PC DNA (and therefore lower total [EP_{40}]) are limited by the association of ES_{18} into the ROO filament, hence contributing little to defining the DNA cleavage rate constant. Data from the other experimental data sets (*i.e.* Data Sets 5-6) measure steps including those after DNA cleavage and are limited by the slower rate constant for dissociation of EP_{18} from ROO filament, therefore also do not help to define the upper limit of the DNA cleavage rate constant.

Finally, release of cleaved reporter DNA (18M-1) from SgrAI, also referred to here as product release (k_7), was fit to 3-10 s^{-1}, but really was constrained by the data only to a lower limit of 0.4-1.0 s^{-1}, depending on the model (**Table 5, Fig. S5F**). This is likely due to the fact that earlier steps limit the reaction kinetics measured in these experiments, such that they provide little data on the product release step itself. The estimated lower limit of 0.4-1.0 s^{-1} is similar to the estimate for the dissociation of uncleaved reporter DNA (18M-1) from SgrAI of 0.6 s^{-1}, which is based on the measured equilibrium constant and estimates of the forward, diffusion limited, association rate constant (see Supporting Information).

Pathway of reporter DNA bound SgrAI in DNA cleavage reactions

A simulation was done to follow ES_{18} and EP_{18} (SgrAI bound to the reporter DNA 18M-1) during the course of the DNA cleavage reaction. **Figure S7A** shows the simulation using model ***"Full Pathway 4BM"*** and its fitted rate constants (**Tables 5-6**) and plots the concentrations of ES_{18} (or EP_{18}) alone (green), or in ROO filaments of size 2 (red), 3 (cyan) or 4 (blue), and scaled for the number of ES_{18} (or EP_{18}) present. These are plotted for several different initial conditions, differing in the concentration of total PC DNA (which changes the concentration of total EP_{40}), and all with 10 nM

reporter DNA (18M-1) and 1 μM SgrAI starting concentrations.

Most of the ES_{18} (and/or EP_{18}) was found to be isolated from EP_{40} (*i.e.* not in an ROO filament) during most of the reaction time, and **Figure S7B** shows that the majority of these are ES_{18} (blue lines), rather than EP_{18}. Because product release (dissociation of cleaved 18M-1 DNA from SgrAI, k_7) is fast (**Table 6, Fig. S5F**), very little SgrAI is bound to cleaved 18M-1 DNA (*i.e.* EP_{18} plotted in red, **Fig. S7B**) is found. Most of the SgrAI bound to 18M-1 DNA is bound to uncleaved DNA (*i.e.* ES_{18}), requiring association with EP_{40} to accelerate DNA cleavage, or alternatively, in time, to cleave DNA itself using the unaccelerated DNA cleavage with rate constant of $9x10^{-4}$ s^{-1} (k_8, **Table 6**).

Figure S7C shows the percent (relative to total 18M-1 DNA) that is in a ROO filament with more than one copy of ES_{18} and/or EP_{18}. As can be seen, this species occurs in only a very low amount, 0.08% or less. This simulation was done to determine whether or not FRET between multiple copies of Flo-18M-1-Rox bound to SgrAI in the same ROO filament should be considered in the modeling, however due to its low quantity, this adjustment was not necessary.

Tests for evidence of cooperativity in models

To see if the models such as ***"Filament Assembly 5EO"*** could reproduce the cooperativity of ROO filament formation seen in **Fig. 3** (see Supporting Information and **Fig. S8**), the fraction of SgrAI/DNA complexes in ROO filament were predicted, as well as the predicted FRET signal (even in a modified model allowing ROO filaments up to 9mers, see Supporting Information and **Tables S15-S16**) at different total [EP_{40}]. When plotted vs. total [EP_{40}] and fit to the Hill equation, no cooperativity is evident (**Fig. S8A-B)**. Hence the models derived here do not intrinsically result in ROO filament formation that is cooperative on total [EP_{40}].

To introduce cooperativity into a model, the ***"Full Pathway 4BM"*** model was altered to include serially slower dissociation rate constants with increasing ROO filament size (see Supporting Information). This could be imagined to result from a greater number of favorable interactions made between the SgrAI/DNA complexes in the ROO filament when more complexes are present. The resulting effect on the quality of the fits is shown in **Table S2**. As can be seen, the fits for cooperativity factors of 5 or below are similar but very much poorer than with a cooperativity factor of 10. In particular, the simulations of data from Data Set 5 (which is most influenced by ROO filament dissociation rates) fit most poorly with larger cooperativity factors and hence slower ROO filament dissociation rates.

DISCUSSION

In this two-part work, measurements of various equilibria and reactions were made in order to better understand the run-on oligomer (ROO) filament mechanism used by SgrAI in DNA cleavage. Most of these measurements use FRET to measure rates of association of SgrAI/DNA complexes and rates of DNA cleavage and release. FRET was also used to measure the concentration dependence of assembly of SgrAI/DNA complexes into ROO filaments, in order to obtain measures of affinity and cooperativity (**Table 1**). This latter measurement involves titrating a low concentration of one type of SgrAI/DNA complex with increasing concentrations of another, and measuring the signal that arises when they are in close proximity to each other. For the kinetic measurements, various reaction schemes were used in order to isolate particular steps in the reaction pathways, and/or to allow for simplified models with fewer rate constants to be fit. In this way, models of increasing complexity could be fit to data sets with greater confidence. Model fitting also allowed for the investigation of cooperativity, ROO filament growth mechanisms, and trapping of cleaved DNA.

This second part of the two-part work focuses on global fitting of DNA cleavage data to test various models and extract microscopic rate constants for each step of the reaction pathway. **Table 2** summarizes the different models used in global data fitting in the current work, and **Table 3** and **Tables 5-6** summarize their fitted rate constants as well as their estimated error boundaries, which are also summarized graphically in **Fig. S5**. **Table 8** gives the final best estimates of these rate constants considering all measurements including those in Part 1 (18).

Run-On Oligomer Filament Growth Formation

The different ROO filament growth and dissolution mechanisms (*i.e.* "ends only" vs. "breaks in the middle", **Table 2**) were tested and resulted in very similar fitted rate constants (compare rate

constants and error boundaries in **Fig. S5**). However, at least with the self-association of EP_{40}, we argue in Part 1 (18) that the three-dimensional structure and lack of cooperativity seen in association measurements suggest that the "breaks in the middle" and not the "ends only" model is most consistent with this data. In the "breaks in the middle" model, ROO filaments may form from other ROO filaments and importantly, ROO filaments may break into smaller ROO filaments by the breaking of any contact between any adjacent SgrAI/DNA complexes. Hence in the current work, we favor ***"Filament Assembly 5BM"*** for fitting of Data Set 4 data, and ***"Full Pathway 4BM"*** for fitting data from Data Sets 5-7, since these both contain the "breaks in the middle" mechanism and for the largest ROO filaments possible to model.

Table 8 summarizes rate constants from the favored model (i.e. ***"Full Pathway 4BM"***). Also included in **Table 8** are estimates of error on each rate constant, determined from the quality of fit of to the experimental data. However, because the association and dissociation of EP_{40} was less constrained by the data used in this model error boundaries for rate constants k_4 and k_{-4} are instead taken from Part 1 (18), which measure only these steps and give better estimates of these rate constants. The rate constants of **Table 8** and their boundaries justify some assumptions and simplifications in our modeling: first, our modeling precluded ROO filaments larger than 4 or 5 SgrAI/DNA complexes, but the extracted rate constants and simulations indicate that larger ROO filaments are not predicted for the concentrations of DNA used in the assays (18). Secondly, again due to limitations in modeling, it was necessary in certain models (***"Full Pathway 4BM"*** only) to make the assumption that when DNA cleavage occurs within an ROO filament, this occurs for all SgrAI/DNA complexes (in this case, ES_{18}) prior to ROO filament dissociation *(i.e.* we model simultaneous DNA cleavage in any ROO filament with more than one ES_{18}). This assumption is justified by the limits on ROO filament dissociation and DNA cleavage rate constants, showing that DNA cleavage is significantly faster than ROO filament dissociation. In addition, the fraction of ROO filament with greater than one ES_{18} and/or EP_{18} is very small (**Fig. S7C**).

Cooperativity

Most measures of cooperativity, as described in Results are either inconclusive or indicate no cooperativity on PC DNA concentration (or total [EP_{40}]) in ROO filament assembly or DNA cleavage. These tests include: 1) Hill plots of Data Set 5 and Data Set 7 data (**Figs. 5C-D, 6B**), 2) simulations of ROO filament concentrations and of FRET signal (**Fig. S8)**, 3) introducing cooperativity into a ***"Full Pathway 4BM"*** to fit data from Data Sets 5-7 (**Table S2),** 4) FRET titrations of ES_{40} with EP_{40} (18)(**Table 1**), and finally 5) simulation of ROO filament size distributions when cooperativity is included and comparing to that found by EM (18). However, one measure did show cooperativity in binding SgrAI/DNA complexes to ROO filament, specifically, of ES_{18} to EP_{40} to form the ROO filament (**Fig. 3B**). This uses FRET between Rox-18M-1 bound to SgrAI and Flo-PC bound to SgrAI (**Fig. 2A**). A fit of the data to the Hill equation provides a Hill coefficient, N, of 2.5±0.3 (**Table 1**). The Hill coefficient, N, is a measure of cooperativity and N>1 indicates positive cooperativity. A Hill coefficient of 2.5±0.3 can be interpreted as ES_{18} binding cooperatively with 2-3 copies of EP_{40}. Though we feel from analysis of the CryoEM structure of the ROO filament that association of SgrAI/DNA complexes into the ROO filament should not be cooperative, and the similar FRET titration ES_{40} with EP_{40} shows no evidence of cooperativity (18), the reduced number of contacts from the shortened 18M-1 flanking DNA (relative to PC DNA), may require additional EP_{40} binding to stabilize the ROO filament. Our attempts to see if our models, which do not have cooperativity specifically built in, would lead to simulated data that would show a Hill coefficient greater than 1, did not (**Fig. S8**). Introduction of such cooperativity to models in the form of decreasing dissociation rate constants with longer ROO filament fit equally well to the observed experimental data (**Table S2**) when the cooperativity was low but deviate significantly when higher (**Table S2**). Therefore, our experimental kinetic data is consistent with some level of cooperativity in binding ES_{18} to EP_{40}, although it cannot conclusively distinguish between a low degree and a complete absence of cooperativity. It should be noted that the DNA cleavage rate is dependent on the concentration of SgrAI/DNA complexes, since association of these complexes must occur prior to activation, and therefore cooperative in that sense, but the reactions

are not cooperative in terms of the classic definition defined by the Hill equation.

Interpretations and significance of fitted rate constants

From the above analyses, several important conclusions can be drawn for solution reactions done with SgrAI *in vitro*. First, because ES_{18} (SgrAI bound to 18M-1 DNA) does not self-associate at the reaction temperature, activation of DNA cleavage in ES_{18} requires the addition of EP_{40} (SgrAI bound to self-annealed PC DNA). This association is rate limiting at concentrations of total EP_{40} below 250 nM, and therefore the overall rate of DNA cleavage increases with increasing total EP_{40} concentration in this range (13,16). The association is rate limiting due to the relatively slow association rate constant, $k_5 \sim 1\text{-}2x10^5$ M^{-1} s^{-1} (**Table 8**) which is approximately three to four orders of magnitude slower than diffusion limited (19,20).

At higher concentrations of EP_{40}, downstream steps limit the overall reaction rate to a greater degree. DNA cleavage is fast within the ROO filament, $k_6 = 0.8$ s^{-1} (**Table 2**), and is three orders of magnitude faster than in isolated (*i.e*. not in an ROO filament) ES_{18} ($k_8 = 9x10^{-4}$ s^{-1}, **Table 2**). Further, the accelerated DNA cleavage rate constant is now comparable to that measured for other restriction endonucleases including EcoRV (21) (0.6±0.06 s^{-1}) and EcoRI (12)(0.34±0.07 s^{-1}). Dissociation of ES_{18} from EP_{40} in the ROO filament is estimated to occur with a rate constant k_{-5} of 0.08 s^{-1} (**Table 8)**. This dissociation rate constant is slower than the DNA cleavage rate constant by a factor of 10, indicating that upon association with EP_{40}, the ES_{18} is more likely to cleave DNA than to dissociate, resulting in a form of commitment and efficiency in the reaction.

One aspect of the reaction mechanism determined from this work is the relatively fast association and dissociation of SgrAI/DNA complexes from the ROO filament, preventing long-term trapping. Simulations to estimate the time ES_{18} and EP_{18} spend in the ROO filament shows 200-300 sec or less (**Fig. S7A**). Following dissociation of EP_{18} from the ROO filament, product release (dissociation of cleaved 18M-1 from SgrAI) appears to be very fast, and only a lower limit of its rate constant ($k_7 > 0.4$ s^{-1}, **Table 2**) was possible to determine. Hence, release of cleaved DNA in this scenario is not rate limiting. The shorter DNA 18M-1 was used to prevent the rebinding of cleaved 18M-1 DNA thereby making its dissociation from SgrAI irreversible (since this DNA when cleaved dissociates irreversibly into separated single strands). The *in vivo* situation is distinct in this respect, as SgrAI cleavage recognition sites will be present in longer DNA that do not dissociate into single strands. Still, trapping should not occur given that rapid association and dissociation of SgrAI/DNA complexes from the ROO filament, and the "breaks in the middle" mechanism ensures even those complexes buried in the filament access to dissociation.

An important result that the association of SgrAI/DNA complexes (*i.e.* ES_{18} and EP_{40} in our reactions) is rate limiting is significant. Given likely concentrations of DNA in the cell (estimated as 3 nM for 1 copy per cell for 1 DNA copy), association of SgrAI/DNA complexes on separate DNA molecules is predicted to be very slow ($2x10^5$ M^{-1} s^{-1} x $3x10^{-9}$ M x $3x10^{-9}$ M = $1.8x10^{-12}$ M/s or $1.8x10^{-3}$ nM/s). However, when present on the same DNA molecule, association is greatly accelerated by local concentration effects. Each 10-fold increase in concentration due to local concentration effects increases the association rate 100 fold. Hence, the combination of the slow, second order rate limiting association rate constant, and local concentration effects, results in sequestration of activated DNA cleavage by SgrAI to sites within the same DNA molecule. This would result in rapid cleavage of both primary and secondary sites in invading phage DNA, with minimal damage to the host genome, and in particular, to likely unmethylated and unprotected secondary sites.

Conclusions

Only recently has filament formation by non-ATP or GTPases been appreciated. New imaging technologies have allowed for large-scale screening of protein localization in cells, and have revealed filament formation by many metabolic and other enzymes, sometimes coinciding with particular phases of the cell cycle, certain stress conditions, or as part of signaling pathways (1-7,22-29). Run-on oligomers, or ROO filaments, are by definition filaments, although not all ROO filaments form filaments as large and as stable as others. The SgrAI ROO filament has been observed to form filaments composed of up to 20 or more SgrAI/DNA complexes *in vitro* (16,30). These may be more limited in size *in vivo* (to number of recognition sites in DNA, usually 10-20 per phage genome including both primary and secondary sites) and may be short-

lived. Much larger filaments (several microns in length) formed by other enzymes can be visualized in cells, and have been found to be stable for minutes to hours (3-5,7,22-25). Only for a handful of such enzymes is the effect (*i.e.* activating or inhibiting) on enzymatic activity known (27,28,31-36). However, the particular *advantages* of forming a filament to control enzyme behavior is largely unexplored. Functions for filament formation have been proposed in the various systems in which they have been found including: sequestration of enzyme activity, rapid enzyme activation or inhibition, storage, fine tune buffering of metabolic activity, in forming cytoskeleton-like structures, protein stabilization, developmental switching, rapid cell proliferation, stress coping, metabolic channeling, and finally intracellular transportation (2,6,16). However, few studies have investigated the *kinetics* of filament or ROO filament formation and none with the level of detail here.

Only one other theoretical model to understand the enzyme kinetics of enzyme filament formation and its function in enzyme turnover has been published (27), however, this model (of CTP synthase assembly) is derived from theory and based on several assumptions including positive cooperativity, the presence of a nucleation step, and growth limited to only the ends of filaments. This model is not a simulation, but a derived mathematical equation, with some coarse data fitting (6 data points from *in vivo* data imaging). The authors conclude that the filaments act as a reservoir and buffer to maintain a constant concentration of the enzyme in the cell, which can respond to the environment to increase or decrease that buffered concentration rapidly as needed (for example, in starvation conditions). Our modeling differs in that it is an explicit simulation rather than a singularly derived equation, and we test the assumptions of cooperativity, nucleation, and growth kinetics. We also use a considerably larger set of experimental data and derive the individual microscopic rate constants, not only for ROO filament assembly, but for enzyme catalysis and product release as well. These models and derived microscopic rate constants will be used in simulations to investigate different starting conditions and conditions *in vivo* in future works.

In conclusion, our study quantifies individual steps and affinities in the assembly of ROO filaments, DNA cleavage, filament disassembly, and release of product (cleaved DNA) from the enzyme. We test various models for ROO filament assembly and find that cooperativity is not required to fit the experimental data, though some cooperativity with certain shorter DNA substrates may be present. In addition, our data are consistent with different growth mechanisms (ends only or breaking in the middle), but we find that the lack of observed cooperativity combined with structural analysis of the ROO filament is most consistent with a model allowing for disassembly at any junction within the filament. We also find that DNA cleavage is accelerated ~1,000 fold to a rate constant of approximately 0.8 s^{-1}. This is much faster than dissociation of the ROO filament, though ROO filament dissociation is fast enough to prevent significant trapping of product complexes. Importantly, we propose that the slow, second order rate limiting association step to form the ROO filament serves the purpose of sequestering activated DNA cleavage, particularly cleavage of secondary sites, on invading DNA and away from damaging the host genome.

EXPERIMENTAL PROCEDURES

Protein and DNA preparation

SgrAI enzyme and DNA were prepared as described (18). The sequences of DNA oligonucleotides used are:

18M-1-top 5'-GAGTCCA|CCGGTGCTGAG-3'
18M-1-bot 3'-CTCAGGTGGCC|ACGACTC-5'

PC-top 5'-GATGCGTGGGTCTTCACA -3'
PC-bot 3'-CTACGCACCCAGAAGTGTGGCC-5'

Data Set 5: Fluorescence measurements with doubly labeled 18M-1 (Flo-8M-1-Rox)

Doubly labeled 18M-1 (Flo-18M-1-Rox) was prepared by annealing single stranded Flo-18M-1-bot (possessing a covalently linked 5' fluorescein (6-FAM or 6-carboxyfluorescein connected to the 5' phosphate via a trans-4-amino cyclohexanol linker, **Fig. S1A**, excitation=495 nm, emission=520nm), and single stranded Rox-18M-1-top (possessing a covalently linked 5' rhodamine-X or 5(6)-carboxy-X-rhodamine connected to the 5'phosphate via a 6-amino hexan-1-ol linker, **Fig. S1B**, excitation=575 nm, emission=603 nm), both prepared synthetically from a commercial source (Sigma-Genosys, Inc.). Reactions were carried out in 1.5 ml volume in a 2

ml cuvette with constant stirring and consisted of 10 nM Flo-18M-1-Rox, 50 nM - 1 μM SgrAI, and 0-1 μM unlabeled PC DNA in buffer A (50 mM Tris-HCl, 150 mM NaCl, 10% glycerol, 1 mM DTT, pH 8.0) supplemented with 10 mM $MgCl_2$, and at 25°C. Fluorescence measurements were taken using a ISS PC-1 fluorimeter with 495 nm excitation and emission monitored at 520 nm emission via monochromator and 1 mm (8 nm spectral width) slits. Intensity measurements were taken in 0.1 msec readings and averaged over 10 iterations for readings approximately every 1.1 sec. After DNA cleavage, dissociation from SgrAI and strand separation, FRET between the Flo and Rox labels is lost, resulting in an increase in Flo emission (**Fig. S2A**).

Data Set 4 & 6: Fluorescence measurements with Rox labeled 18M-1 (Rox-18M-1) and Flo labeled PC DNA (Flo-PC)

This data was measured as described (18) for Data Sets 1-3 in that work, but with Rox labeled 18M-1 (Rox-18M-1) (Rox-18M-1-top annealed to unlabeled 18M-1-bot) and Flo-PC (Flo labeled PC top and unlabeled PC bot). In the case of Data Set 4, SgrAI was added last to the mixture of DNA in buffer A (with no divalent cation) at 25°C (1.5 ml total volume), and emission was followed through the 590 nm cut-on filter (measuring Rox and Flo emission signals) and at 585 nm (to monitor Flo emission). Data Set 6 differed in the inclusion of 10 mM $MgCl_2$, adding Rox-18M-1 last to the reaction, and following the Flo emission at 520 nm. The corrected filter (CF) data used in data fitting was calculated as follows:

Data Set 6:

$$Correction\ factor\ ratio\ C = \frac{I(Flo-PC)_{590cof}}{I(Flo-PC)_{520}}$$

$$Corrected\ Filter\ Data\ (reaction,t) = I(reaction,t)_{590cof} - C \times I(reaction,t)_{585}$$

Data Set 4:

$$Correction\ factor\ ratio\ C = \frac{I(Flo-PC)_{590cof}}{I(Flo-PC)_{585}}$$

$$Corrected\ Filter\ Data\ (reaction,t) = I(reaction,t)_{590cof} - C \times I(reaction,t)_{585}$$

Where $I(Flo-PC)_{590cof}$, $I(Flo-PC)_{585}$, and $I(Flo-PC)_{585}$ are the intensities from a solution containing only Flo-PC and measured through the 590 cut-on filter, and using a monochromater at 520 nm, and at 585 nm, respectively.

Data Set 7: DNA cleavage reactions using Flo-18M-1-Rox and denaturing PAGE

Doubly labeled 18M-1 (Flo-18M-1-Rox) was prepared as described above for Data Set 5. Reactions were performed in 100 μl total volume and consisted of 50 nM Flo-18M-1-Rox, 1 μM SgrAI, and 0-1 μM unlabeled PC DNA in buffer A at 25°C in 100 μl total volume. Reactions were initiated by mixing solution A (containing Flo-18M-1-Rox) with solution B (containing SgrAI and PC DNA) at time=0. At various times after mixing, 5 μl aliquots were removed and quenched in a separate tube with an equal volume of quench solution (containing 80% formamide, 50 mM EDTA, 0.05% bromophenol blue, 0.05% xylene cyanol). An initial 2.5 μl aliquot was taken from each solution (A and B) before mixing to represent time = 0 sec. Aliquots were analyzed by electrophoresing on 20% acrylamide (19:1 acrylamide:bis-acrylamide) gels containing 4 M urea and 1x TBE (89 mM Tris base, 89 mM boric acid, 2 mM EDTA), and scanned with a Pharos phosphoimager (BioRad, Inc.) for Flo and Rox fluorescent bands. Bands were integrated for their intensity using the software ImageLab (BioRad, Inc.). The percentage of DNA cleaved was calculated by dividing the intensity of the cleaved DNA band over the sum of the cleaved and uncleaved DNA bands. This data, as a function of time after initiation, was used in subsequent analyses and data fitting.

FRET Titrations to measure association of DNA bound SgrAI into ROO filament

Titrations were performed with 50 nM Rox-18M-1, 2-4 μM SgrAI, and varied concentrations of Flo-PC DNA or Flo-18M-1 in buffer A supplied with 10 mM $CaCl_2$, in 1.5 ml total and maintained at 25°C. Care was taken to ensure an excess of SgrAI over that of the DNA. Excitation was done using 498 nm, and emission spectra collected (in a ratio with excitation) following two minutes incubation with constant stirring after each addition of Flo-DNA. Flo labeled DNA was a mixture of labeled and unlabeled (1:9 Flo-PC:PC and 1:4 Flo-18M-1:18M-1).

Resulting spectra were corrected for dilution of the added DNA, for Flo emission (using a reference Flo-DNA only spectrum scaled by relative emission at 570 nm), and for Rox emission due to absorbance at 498 nm (using the spectrum before added Flo-DNA). The resulting average emissions at 602-612 nm (or 603-613 nm) were plotted vs. concentration of Flo-DNA and fit to the Hill equation (see below). In a separate experiment, the titration was repeated without the presence of divalent cations, using 200 nM Rox-18M-1, 2 μM SgrAI, and 2 μM Flo-PC. After recording the spectrum, 10 mM $MgCl_2$ was added. Spectra were recorded 15 and 30 minutes later, and the corrected spectrum calculated for evidence of residual FRET (to test for trapping of the Rox-18M-1 in the oligomer).

Analytical Fitting of Data

The Flo emission (Data Set 5) and DNA cleavage (Data Set 7) data were fit using the software Kaleidagraph (Synergy Software) to a single exponential function and a rate constant determined:

$$y = a + b \times \left(1 - e^{-k(t-c)}\right)$$

where y is the parameter to be fit (increase in FRET signal, Fluorescence, or Percentage of cleaved DNA), a and b are constants to be fit in each reaction, k is the rate constant, t is time, and c is a time correction for data where initiation is later than time=0.

The titration data were fit using Kaleidagraph (Synergy Software) and the Hill equation:

$$y = a + b \times \left(\frac{[EP_{40}]^N}{(K_{1/2})^N + [EP_{40}]^N}\right)$$

Where y is the average of the intensities at 602-612 nm (or 603-613 nm) of the fluorescence emission at each total concentration of EP_{40} (equal to ½ the concentration of added PC DNA), $K_{1/2}$ is the concentration of EP_{40} (total) where the average emission intensity is half maximal, and N is the Hill coefficient (a measure of the cooperativity of the reaction).

Global Data Fitting

Global data fitting was performed with Kintek Global Kinetic Explorer version 6.2.170301 (Kintek Global Kinetic Explorer Corp.)(37-39). Data fitting was as described in Part 1 (18) and equations for each model are provided in the Supporting Information.

Error Analysis

The Fitspace module of Kintek GKE (39) was used to determine error boundaries for fitted rate constants at the 0.95 χ^2 threshold, meaning that values within these boundaries result in χ^2, the sum of the squares of residuals between experimental and fitted values, less than or equal to the (minimum or best χ^2)/0.95 (39). In some cases, limits on parameters tested were imposed as described. In the case of models using Data Sets 5-7 (see **Table 2**), weighting was used to allow each independent data set (each "experiment" in Kintek GKE) equal weighting in the Fitspace calculation (to avoid over-weighting of those data sets with higher χ^2). Weights were calculated as 1000/(χ^2 for that particular data set) for each data set.

Data Simulations

Where indicated, rate constants from Kintek GKE data fitting were used with new or existing models to predict concentrations of different reaction species as a function of time in the reaction, including at equilibrium, in order to address specific questions or to compare to other experimental data. In such cases, the equations used for the model and the rate constants being used are given (or reference to previously presented models and rate constants given). For the introduction of cooperativity into models, the dissociation rate constants for SgrAI/DNA complexes from ROO filament were made serially slower by a factor (X) with larger ROO filament. For example, if the rate constant for dissociation is 0.08 s^{-1}, and X is 1.5, then the dissociation of SgrAI/DNA complexes from a ROO filament is 0.08 s^{-1} when the ROO filament is composed of two SgrAI/DNA complexes, 0.08/1.5 s^{-1} when composed of three SgrAI/DNA complexes, and (0.08/(1.5)^2) s^{-1} when composed of four SgrAI/DNA complexes.

Acknowledgments: Research reported in this publication was supported by the National Science Foundation under Grant No. MCB-1410355, the Office of the Director, National Institutes of Health of the National Institutes of Health under award number S10OD013237, and by the National Institute of General Medical Sciences of the National Institutes of Health under award number T32GM008659 (to JLS). The contents of this publication are

solely the responsibility of the authors and do not necessarily represent the official views of NIGMS, NIH or NSF. We would also like to thank Robert M. Blumenthal for helpful discussions.

Conflict of Interest: The authors declare that they have no conflicts of interest with the contents of this article.

REFERENCES

1. Barry, R. M., and Gitai, Z. (2011) Self-assembling enzymes and the origins of the cytoskeleton. *Current opinion in microbiology* **14**, 704-711
2. Liu, J. L. (2016) The Cytoophidium and Its Kind: Filamentation and Compartmentation of Metabolic Enzymes. *Annu Rev Cell Dev Biol* **32**, 349-372
3. Narayanaswamy, R., Levy, M., Tsechansky, M., Stovall, G. M., O'Connell, J. D., Mirrielees, J., Ellington, A. D., and Marcotte, E. M. (2009) Widespread reorganization of metabolic enzymes into reversible assemblies upon nutrient starvation. *Proc Natl Acad Sci U S A* **106**, 10147-10152
4. Werner, J. N., Chen, E. Y., Guberman, J. M., Zippilli, A. R., Irgon, J. J., and Gitai, Z. (2009) Quantitative genome-scale analysis of protein localization in an asymmetric bacterium. *Proc Natl Acad Sci U S A* **106**, 7858-7863
5. Noree, C., Sato, B. K., Broyer, R. M., and Wilhelm, J. E. (2010) Identification of novel filament-forming proteins in Saccharomyces cerevisiae and Drosophila melanogaster. *The Journal of cell biology* **190**, 541-551
6. O'Connell, J. D., Zhao, A., Ellington, A. D., and Marcotte, E. M. (2012) Dynamic reorganization of metabolic enzymes into intracellular bodies. *Annu Rev Cell Dev Biol* **28**, 89-111
7. Suresh, H. G., da Silveira Dos Santos, A. X., Kukulski, W., Tyedmers, J., Riezman, H., Bukau, B., and Mogk, A. (2015) Prolonged starvation drives reversible sequestration of lipid biosynthetic enzymes and organelle reorganization in Saccharomyces cerevisiae. *Molecular biology of the cell* **26**, 1601-1615
8. Park, C. K., Stiteler, A. P., Shah, S., Ghare, M. I., Bitinaite, J., and Horton, N. C. (2010) Activation of DNA cleavage by oligomerization of DNA-bound SgrAI. *Biochemistry* **49**, 8818-8830
9. Stern, A., and Sorek, R. (2010) The phage-host arms race: shaping the evolution of microbes. *Bioessays* **33**, 43-51
10. Bitinaite, J., Mitkaite, G., Dauksaite, V., Jakubauskas, A., Timinskas, A., Vaisvila, R., Lubys, A., and Janulaitis, A. (2002) Evolutionary relationship of Alw26I, Eco31I and Esp3I, restriction endonucleases that recognise overlapping sequences. *Molecular Genetics & Genomics: MGG* **267**, 664-672
11. Hingorani-Varma, K., and Bitinaite, J. (2003) Kinetic analysis of the coordinated interaction of SgrAI restriction endonuclease with different DNA targets. *J Biol Chem* **278**, 40392-40399
12. Lesser, D. R., Kurpiewski, M. R., and Jen-Jacobson, L. (1990) The energetic basis of specificity in the Eco RI endonuclease--DNA interaction. *Science* **250**, 776-786.
13. Shah, S., Sanchez, J., Stewart, A., Piperakis, M. M., Cosstick, R., Nichols, C., Park, C. K., Ma, X., Wysocki, V., Bitinaite, J., and Horton, N. C. (2015) Probing the Run-On Oligomer of Activated SgrAI Bound to DNA. *PLoS One* **10**, e0124783
14. Dunten, P. W., Little, E. J., Gregory, M. T., Manohar, V. M., Dalton, M., Hough, D., Bitinaite, J., and Horton, N. C. (2008) The structure of SgrAI bound to DNA; recognition of an 8 base pair target. *Nucleic Acids Res* **36**, 5405-5416
15. Little, E. J., Dunten, P. W., Bitinaite, J., and Horton, N. C. (2011) New clues in the allosteric activation of DNA cleavage by SgrAI: structures of SgrAI bound to cleaved primary-site DNA and uncleaved secondary-site DNA. *Acta Crystallogr D Biol Crystallogr* **67**, 67-74
16. Lyumkis, D., Talley, H., Stewart, A., Shah, S., Park, C. K., Tama, F., Potter, C. S., Carragher, B., and Horton, N. C. (2013) Allosteric regulation of DNA cleavage and sequence-specificity through run-on oligomerization. *Structure* **21**, 1848-1858
17. Dryden, D. T. (2013) The architecture of restriction enzymes. *Structure* **21**, 1720-1721
18. Park, C. K., Sanchez, J. L., Barahona, C. J., Basantes, L. E., Sanchez, J., Hernandez, C., and Horton, N. C. (2018) The Run-On Oligomer Filament Enzyme Mechanism of SgrAI. Part 1: Assembly Kinetics of the Run-On Oligomer Filament. *Submitted for publication*
19. Alberty, R., and GG, H. (1958) Application of the Theory of Diffusion-controlled Reactions to Enzyme Kinetics. *J. Phys. Chem.* **62**, 154-159
20. Eigen, M., and Hammes, G. G. (1963) Elementary Steps in Enzyme Reactions (as Studied by Relaxation Spectrometry). *Adv Enzymol Relat Subj Biochem* **25**, 1-38
21. Sam, M. D., and Perona, J. J. (1999) Mn2+-dependent catalysis by restriction enzymes: pre-steady-state analysis of EcoRV endonuclease reveals burst kinetics and the origins of reduced ativity. *J. Am. Chem. Soc.* **121**, 1444-1447

22. Shen, Q.-J., Kassim, H., Huang, Y., Li, H., Zhang, J., Li, G., Wang, P.-Y., Ye, F., and Liu, J.-L. (2016) Filamentation of Metabolic Enzymes in *Saccharomyces cerevisiae*. *Journal of Genetics and Genomics* **43**, 393-404
23. Schmitt, D. L., Cheng, Y. J., Park, J., and An, S. (2016) Sequestration-Mediated Downregulation of de Novo Purine Biosynthesis by AMPK. *ACS Chem Biol* **11**, 1917-1924
24. Zaganjor, E., Spinelli, J. B., and Haigis, M. C. (2017) Strength in numbers: Phosphofructokinase polymerization prevails in the liver. *The Journal of cell biology* **216**, 2239-2241
25. Prouteau, M., Desfosses, A., Sieben, C., Bourgoint, C., Lydia Mozaffari, N., Demurtas, D., Mitra, A. K., Guichard, P., Manley, S., and Loewith, R. (2017) TORC1 organized in inhibited domains (TOROIDs) regulate TORC1 activity. *Nature* **550**, 265-269
26. Vajjhala, P. R., Ve, T., Bentham, A., Stacey, K. J., and Kobe, B. (2017) The molecular mechanisms of signaling by cooperative assembly formation in innate immunity pathways. *Mol Immunol* **86**, 23-37
27. Aughey, G. N., Grice, S. J., Shen, Q. J., Xu, Y., Chang, C. C., Azzam, G., Wang, P. Y., Freeman-Mills, L., Pai, L. M., Sung, L. Y., Yan, J., and Liu, J. L. (2014) Nucleotide synthesis is regulated by cytoophidium formation during neurodevelopment and adaptive metabolism. *Biol Open* **3**, 1045-1056
28. Petrovska, I., Nuske, E., Munder, M. C., Kulasegaran, G., Malinovska, L., Kroschwald, S., Richter, D., Fahmy, K., Gibson, K., Verbavatz, J. M., and Alberti, S. (2014) Filament formation by metabolic enzymes is a specific adaptation to an advanced state of cellular starvation. *Elife* **3**, e02409
29. An, S., Kumar, R., Sheets, E. D., and Benkovic, S. J. (2008) Reversible compartmentalization of de novo purine biosynthetic complexes in living cells. *Science* **320**, 103-106
30. Ma, X., Shah, S., Zhou, M., Park, C. K., Wysocki, V. H., and Horton, N. C. (2013) Structural Analysis of Activated SgrAI-DNA Oligomers Using Ion Mobility Mass Spectrometry. *Biochemistry* **52**, 4373-4381
31. Kim, C. W., Moon, Y. A., Park, S. W., Cheng, D., Kwon, H. J., and Horton, J. D. (2010) Induced polymerization of mammalian acetyl-CoA carboxylase by MIG12 provides a tertiary level of regulation of fatty acid synthesis. *Proc Natl Acad Sci U S A* **107**, 9626-9631
32. Barry, R. M., Bitbol, A. F., Lorestani, A., Charles, E. J., Habrian, C. H., Hansen, J. M., Li, H. J., Baldwin, E. P., Wingreen, N. S., Kollman, J. M., and Gitai, Z. (2014) Large-scale filament formation inhibits the activity of CTP synthetase. *Elife* **3**, e03638
33. Lynch, E. M., Hicks, D. R., Shepherd, M., Endrizzi, J. A., Maker, A., Hansen, J. M., Barry, R. M., Gitai, Z., Baldwin, E. P., and Kollman, J. M. (2017) Human CTP synthase filament structure reveals the active enzyme conformation. *Nat Struct Mol Biol* **24**, 507-514
34. Korennykh, A. V., Egea, P. F., Korostelev, A. A., Finer-Moore, J., Zhang, C., Shokat, K. M., Stroud, R. M., and Walter, P. (2009) The unfolded protein response signals through high-order assembly of Ire1. *Nature* **457**, 687-693
35. Ghosh, R., Wang, L., Wang, E. S., Perera, B. G., Igbaria, A., Morita, S., Prado, K., Thamsen, M., Caswell, D., Macias, H., Weiberth, K. F., Gliedt, M. J., Alavi, M. V., Hari, S. B., Mitra, A. K., Bhhatarai, B., Schurer, S. C., Snapp, E. L., Gould, D. B., German, M. S., Backes, B. J., Maly, D. J., Oakes, S. A., and Papa, F. R. (2014) Allosteric Inhibition of the IRE1alpha RNase Preserves Cell Viability and Function during Endoplasmic Reticulum Stress. *Cell* **158**, 534-548
36. Li, J., McQuade, T., Siemer, A. B., Napetschnig, J., Moriwaki, K., Hsiao, Y. S., Damko, E., Moquin, D., Walz, T., McDermott, A., Chan, F. K., and Wu, H. (2012) The RIP1/RIP3 necrosome forms a functional amyloid signaling complex required for programmed necrosis. *Cell* **150**, 339-350
37. Johnson, K. A., Simpson, Z.B., Blom, T. (2009) Global Kinetic Explorer: A new computer program for dynamic simulation and fitting of kinetic data. *Analytical Biochemistry* **387**, 20-29
38. Johnson, K. A. (2009) Fitting enzyme kinetic data with KinTek Global Kinetic Explorer. *Methods Enzymol* **467**, 601-626
39. Johnson, K. A., Simpson, Z. B., and Blom, T. (2009) FitSpace explorer: an algorithm to evaluate multidimensional parameter space in fitting kinetic data. *Anal Biochem* **387**, 30-41

TABLES

Table 1. Fitted parameters from Hill analysis of FRET titration data

Reporter[a]	Donor	$K_{1/2}$[b]	Hill Coefficient N
50nM Rox-18M-1	Flo-PC	0.5±0.02 μM	2.5±0.3
50 nM Rox-18M-1	Flo-18M-1	too weak to measure	1.2±0.4
50 nM Rox-40-1[c]	Flo-PC	0.16±0.03 μM	1.1±0.1

[a]See **Fig. 2-3 and Fig. S2**. All performed in the presence of 10 mM $CaCl_2$.

[b]When plotted vs. [SgrAI/Flo-DNA] such as [Flo-ES_{18}] or [Flo-EP_{40}].
[c]From Part 1 (18).

Table 2. Models used in data fitting

Model	Type of data used in fitting[a]	Divalent cofactor	Major steps modeled[b]	Max. size of ROO filament	Filament growth mechanism	Independent or simultaneous cleavage of DNA strands and in ROO filament by separate SgrAI/DNA complexes
Filament Assembly 5EO	**Approach to equilibrium reactions with:** **Data Set 4**: activator (Flo-PC) and reporter DNA (Rox-18M-1) in the absence of DNA cleavage (Rox-ES_{18}+Flo-EP_{40})	None	Self-association of EP_{40}, association of ES_{18} and EP_{40}	5	Ends only[c]	NR[d]
Filament Assembly 5BM				5	Breaks in the middle[e]	NR[d]
Filament Assembly 4EO				4	Ends only[c]	NR[d]
Filament Assembly 4BM				4	Breaks in the middle[e]	NR[d]
Full Pathway 2mers Independent Strand Cleavage	**DNA cleavage reactions with:** **1. Data Set 5**: timed FRET measurements with Rox-18M-1 and Flo-PC (Rox-ES_{18}+Flo-EP_{40}) **2. Data Set 6**: timed FRET measurements with doubly labeled reporter DNA (Flo-18M-1-Rox) and unlabeled activator DNA (PC DNA) **3. Data Set 7:** timed measurements of total DNA cleavage measured by urea-PAGE with doubly labeled reporter DNA (Flo-18M-1-Rox) and unlabeled activator DNA (PC DNA)	10 mM $MgCl_2$	Association of ES_{18} or EP_{18} with EP_{40}, DNA cleavage in ES_{18}, Release of cleaved DNA from EP_{18}	2	NR[f]	Cleavage of each strand is modeled independently
Full Pathway 2mers				2	NR[f]	Simultaneous cleavage of both strands
Full Pathway 3mers				3	NR[f]	Simultaneous cleavage of both strands
Full Pathway 4EO				4	Ends only[c]	simultaneous cleavage of both strands and cleavage by each ES_{18} modeled as independent
Full Pathway 4BM				4	Breaks in the middle[e]	simultaneous cleavage of both strands and cleavage by multiple ES_{18} in the same ROO modeled as occurring simultaneously

[a]EP_{40}, SgrAI bound to self-annealed PC DNA, ES_{18}, SgrAI bound to uncleaved 18M-1 DNA, Flo and Rox refer to the fluorescent labeled attached to the DNA.
[b]Minor steps modeled in all models also include self-association of two PC DNA molecules, association of SgrAI with DNA (18M-1 or self-associated PC DNA), and dissociation of 18M-1 DNA strands following cleavage and dissociation from SgrAI.
[c]"Ends only" refers to models where ROO filaments grow only 1 SgrAI/DNA at a time (EP_{40}, ES_{18}, or EP_{18}), and dissociate only 1 SgrAI/DNA complex at a time and only at the ends of the ROO filament.
[d]NR, not relevant, since ROO filaments never contain more than one ES_{18} in this model.
[e]"Breaks in the middle" refers to models where ROO filaments may form from two species (ROO filaments or individual SgrAI/DNA complexes) containing any number of SgrAI/DNA complexes, and that dissociation of an ROO filament may occur at any junction between adjacent SgrAI/DNA complex in the ROO filament.
[f]NR, not relevant to this model, as these two mechanisms are equivalent for ROO filamentof 3 or fewer SgrAI/DNA complexes.

Table 3. Rate constants for ROO filament assembly from global data fitting of Data Set 4[a]

Reaction Model	EP_{40} + EP_{40} Association Rate Constant (k_4)(M^{-1} s^{-1})	(EP_{40})(EP_{40}) Dissociation Rate Constant (k_{-4})(s^{-1})	EP_{40} + ES_{18} Association Rate Constant (k_5)(M^{-1} s^{-1})	(EP_{40})(ES_{18}) Dissociation Rate Constant (k_{-5})(s^{-1})
Filament Assembly 5EO	$4x10^6$ ($4x10^6$-$7x10^7$)	0.06 (0.012-0.15)	$1.3x10^6$ ($1x10^6$-$6x10^6$)	0.04 (0.03-0.17)
Filament Assembly 5BM	$3x10^6$ ($3x10^6$-$1.5x10^7$)	0.01 ($9x10^{-4}$-0.09)	$1.9x10^6$ ($7x10^5$-$8x10^6$)	0.02 ($5x10^{-5}$-0.2)
Filament Assembly 4EO	$2x10^6$ ($2x10^6$-$1x10^7$)	0.017 (0.002-0.07)	$3x10^6$ ($1.9x10^5$-$5x10^6$)	0.06 (0.05-0.15)
Filament Assembly 4BM	$2x10^6$ ($1x10^6$-$3x10^7$)	0.05 (0.002-0.12)	$1.8x10^6$ ($1.8x10^6$-$1.9x10^6$)	0.08 (0.0015-3)

[a]EP_{40}, SgrAI bound to self-annealed PC DNA, ES_{18}, SgrAI bound to uncleaved 18M-1 DNA. Fitspace boundaries calculated at $0.95*[\chi^2/(\chi^2)_{min}]$ threshold boundary. See **Tables S3-S5** for reactions and equations used in modeling and global data fitting.

Table 4. Quality of fit parameters of global fitting of Data Set 4

Reaction Model	Number of reaction data sets used in global fitting[a]	Number of reaction data points total	Number of fitted parameters (rate constants + baseline/scaling constants)	χ^2/DoF[b]	σ[b]
Filament Assembly 5EO	6	998	7+12=19	2.5	0.021
Filament Assembly 5BM				2.7	0.022
Filament Assembly 4EO				2.5	0.020
Filament Assembly 4BM				2.1	0.019

[a]See **Table S1** for reaction data set details.
[b]χ^2/DoF and σ are as defined by the authors of the modeling software (37,38).

Table 5. Rate constants for ROO filament assembly from global fitting of Data Sets 5-7[a]

Reaction Model	$EP_{40} + EP_{40}$ (k_4) (M^{-1} s^{-1})	$(EP_{40})(EP_{40})$ Dissociation (k_{-4}) (s^{-1})	$EP_{40} + ES_{18}$ or $EP_{40} + EP_{18}$ (k_5) (M^{-1} s^{-1})	$(EP_{40})(ES_{18})$ or $(EP_{40})(EP_{18})$ Dissociation (k_{-5})(s^{-1})
Full Pathway 2mers Independent Strand Cleavage	-	-	$2x10^5$ ($2x10^5$-$3x10^5$)	0.04 (0.04-0.05)
Full Pathway 2mers	-	-	$2x10^5$ ($2x10^5$-$3x10^5$)	0.04 (0.04-0.05)
Full Pathway 3mers	$1.4x10^5$ ($8x10^3$-$5x10^5$)[b]	0.03 ($1.8x10^{-3}$-0.02)[b]	$2x10^5$ ($2x10^5$-$3x10^5$)	0.07 (0.07-0.09)
Full Pathway 4EO	$1.7x10^5$ ($6x10^4$-$7x10^5$)	0.03 (0.017-0.04)	$2.5x10^5$ ($2x10^5$-$3x10^5$)	0.08 (0.07-0.1)
Full Pathway 4BM	$1.2x10^5$ ($6x10^4$–$3x10^5$)	0.03 ($3x10^{-6}$-1.0)	$2x10^5$ ($2x10^5$–$3x10^5$)	0.08 (0.07-0.10)

[a]EP_{40}, SgrAI bound to self-annealed PC DNA, ES_{18}, SgrAI bound to uncleaved 18M-1 DNA, EP_{18}, SgrAI bound to cleaved 18M-1 DNA. Fitspace boundaries calculated at $0.95*[\chi^2/(\chi^2)_{min}]$ threshold boundary. See **Tables S6-S14** for reactions and equations used in modeling and global data fitting.
[b]Overall χ^2 was affected little by values within the tested range.

Table 6. Additional rate constants from global fitting of Data Sets 5-7[a]

Reaction Model	Self-Association of PC DNA forward rate constant (k_1) ($M^{-1}s^{-1}$)	DNA Cleavage within Run-on Oligomer (k_6) (s^{-1})	Dissociation of cleaved 18M-1 from SgrAI (k_7) (s^{-1})	DNA Cleavage by isolated ES_{18} (SgrAI bound to 18M-1) (k_8) (s^{-1})
Full Pathway 2mers Independent Strand Cleavage	$2x10^7$ ($4x10^6$-$8x10^8$)[b]	0.5 (0.2-0.8)[b]	3 (≥0.8)[b]	$7x\ 10^{-4}$ (4×10^{-4} - 10×10^{-4})[b]
Full Pathway 2mers	$2x10^7$ ($5x10^6$-$6x10^8$)[b]	0.5 (0.2-1.0)[b]	3 (≥0.5)[b]	10×10^{-4} (4×10^{-4}-20×10^{-4})[b]
Full Pathway 3mers	$2x10^7$ ($3x10^6$-$6x10^8$)[b]	0.7 (0.3-1.0)[b]	10 (≥1.2)[b]	11×10^{-4} (1.2×10^{-4}-12×10^{-4})[b]
Full Pathway 4EO	$2x10^7$ ($3x10^6$-$5x10^8$)[b]	0.8 (0.3-25)[b] (0.3-1.0)[c]	10 (≥0.4)[b]	5×10^{-4} (3×10^{-4}-10×10^{-4})[b]
Full Pathway 4BM	$2x10^7$ ($1x10^6$-$6x10^8$)[b]	0.8 (0.3-6)[b] (0.4-1.0)[c]	10 (>0.4)[b]	9×10^{-4} ($8x10^{-5}$-20×10^{-4})[b]

[a]See **Tables S6-S14** for reactions and equations used in modeling and global data fitting.
[b]Fitspace $0.95*[\chi^2/(\chi^2)_{min}]$ threshold boundary.

[c]0.99*[χ^2/(χ^2)$_{min}$] threshold boundary.

Table 7. Quality of fit parameters of global fitting of Data Sets 5-7

Reaction Model	Number of reaction data sets used in global fitting	Number of reaction data points total	Number of fitted parameters (rate constants + baseline/scaling constants)	χ^2/DoF[a]	σ[b]
Full Pathway 2mers Independent Strand Cleavage	22	3454	8+50=58	2.3	0.020
Full Pathway 2mers	22	3454	8+50=58	2.7	0.021
Full Pathway 3mers	22	3454	10+50=60	3.3	0.020
Full Pathway 4EO	22	3448	10+50=60	1.7	0.019
Full Pathway 4BM	22	3448	10+50=60	1.8	0.021

[a]DoF is Degrees of Freedom, calculated from the number of data points N and number of fitted parameters. Values of χ^2/DoF closer to 1 indicate better fits.
[b]σ is the "σ with respect to the fit", another measure of how well the experimental data agree with the simulated.

Table 8. Best estimates of global fitted rate constants

Reaction Step[a]	Forward Rate Constant	Reverse Rate Constant
PC DNA+PC DNA=PCDS[b]	$k_1 = 2x10^7$ $M^{-1}s^{-1}$ (10^6 -$6x10^8$ $M^{-1}s^{-1}$)	$k_{-1} = 8$ s^{-1} (0.4-225 s^{-1})
SgrAI+PCDS= EP_{40}[c]	$k_2 = 10^9$ $M^{-1}s^{-1}$	$k_{-2} = 0.06$ sec^{-1}
SgrAI+18M-1 DNA= ES_{18}[c]	$k_3 = 10^9$ $M^{-1}s^{-1}$	$k_{-3} = 0.6$ sec^{-1}
Associations and Dissociations of EP_{40} with EP_{40}	$k_4 = 3x10^5$ $M^{-1}s^{-1}$ ($1.1x10^5$–$7x10^5$ $M^{-1}s^{-1}$)	$k_{-4} = 0.017$ s^{-1} (0.007-0.02 s^{-1})
Associations and Dissociations of ES_{18} with EP_{40} (and EP_{18} with EP_{40})	$k_5 = 2x10^5$ $M^{-1}s^{-1}$ ($2x10^5$–$3x10^5$ $M^{-1}s^{-1}$)	$k_{-5} = 0.08$ s^{-1} (0.07-0.1 s^{-1})
DNA cleavage by ES_{18} in a run-on oligomer filament of any size with EP_{40}	$k_6 = 0.8$ s^{-1} (0.3-6 s^{-1})(0.4-1.0 s^{-1})[d]	NA[e]
Release of cleaved 18M-1 DNA by EP_{18}	$k_7 > 0.4$ s^{-1}	NA[e]
DNA cleavage by ES_{18} not associated with EP_{40}	$k_8 = 9x10^{-4}$ s^{-1} ($8x10^{-5}$-$2x10^{-3}$ s^{-1})	NA[e]

[a]PC DNA, PC DNA, PCDS, self-annealed PC DNA, EP_{40}, SgrAI bound to self-annealed PC DNA, ES_{18}, SgrAI bound to 18M-1 DNA. Association and dissociation rate constants of EP_{40} or ES_{18} (or EP_{18}) with EP_{40} are considered to be independent of the size of the run-on oligomer filament. Ranges given in parentheses correspond to boundaries determined by Fitspace at the 0.95 χ^2 threshold (see Experimental Procedures).
[b]The ratio of the reverse to forward rate constants was constrained to a K_D of 375 nM.
[c]The forward rate constant is assumed to be diffusion limited, with a value of 10^9 $M^{-1}s^{-1}$ (19,20). The reverse rate constant was derived from fitting equilibrium titration data (Part 1 (18), Supporting Information, and previously published values (8)).
[d]Fitspace boundary at 0.99 χ^2 threshold.
[e]NA, not applicable as these rate constants were fixed to 0.

FIGURES

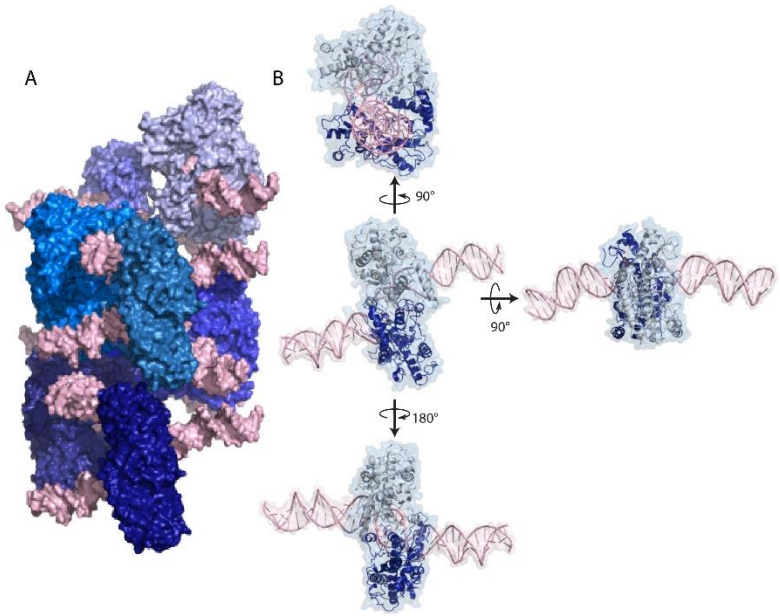

Figure 1. Structure of the SgrAI/DNA run-on oligomer (ROO) filament. A. Surface rendering of ROO filament of SgrAI/DNA complexes (PDB 4C3G). Each SgrAI/DNA is colored a different shade of blue, starting with darker blue at the bottom, and DNA in pink. The oligomer has left-handed helical symmetry with approximately 4 SgrAI/DNA complexes per turn. **B.** Different view of one SgrAI/DNA complex, with the central left orientation the same as the middle front SgrAI/DNA complex in A. Cartoon rendering shown beneath the surface rendering. Each subunit of the SgrAI dimer is shaded differently (light and dark blue). The DNA rendered in cartoon is colored pink.

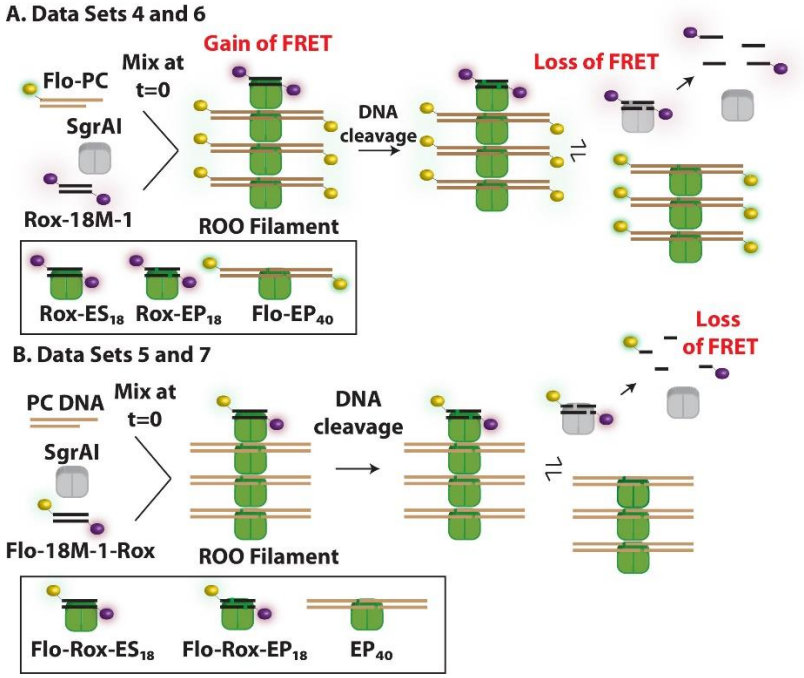

Figure 2. Cartoon representation of reactions schemes. A. Scheme for reactions of Data Sets 4 and 6 and FRET titrations. The change from grey to green filled boxes for the SgrAI dimer indicates activation, presumably via a conformational change. Both the FRET titration and the reactions of Data Set 4 stop before DNA cleavage,

due to absence of Mg^{2+}. **B.** Scheme for reactions of Data Sets 5 and 7. Data Set 5 measures FRET as a function of time after mixing, while Data Set 7 measures the total amount of cleaved Flo and Rox labeled DNA using PAGE and densitometry.

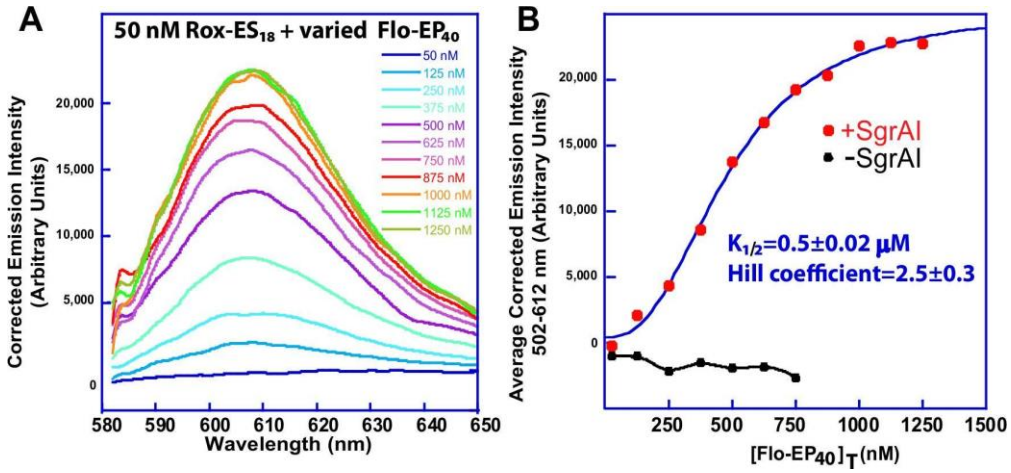

Figure 3. Titration of Rox-18M-1, SgrAI, with Flo-PC DNA in the presence of 10 mM Ca^{2+}. A. 50 nM Rox-18M-1, 2 µM SgrAI, and 10 mM $CaCl_2$ with PC DNA (1:9 Flo-PC:PC) at 25°C. Emission spectra taken with 498 nm excitation, and corrected for Flo emission, dilution, and Rox emission due to absorption at 498 nm. **B.** Average corrected intensities from A (wavelengths 602-612 nm) vs. total EP_{40} concentration (SgrAI bound to self-annealed Flo-PC DNA, consisting of 1:9 Flo-PC:PC)(filled red circles). Fit to Hill plot (blue line) gives $K_{1/2}$=0.50±0.02 µM, Hill coefficient=2.5±0.3, and R=0.99848. Control (black circles and line) performed exactly the same, but without SgrAI.

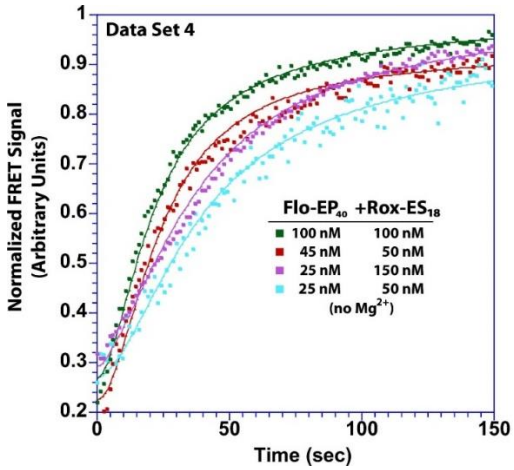

Figure 4. Select reactions from Data Set 4 and *"Filament Assembly 4BM"* simulations. Experimental data (filled circles) and simulated data (lines), for selected reaction data sets. Starting concentrations of Flo-EP_{40} (SgrAI bound to self-annealed Flo-PC DNA) and Rox-ES_{18} (SgrAI bound to Rox-18M-1) as shown.

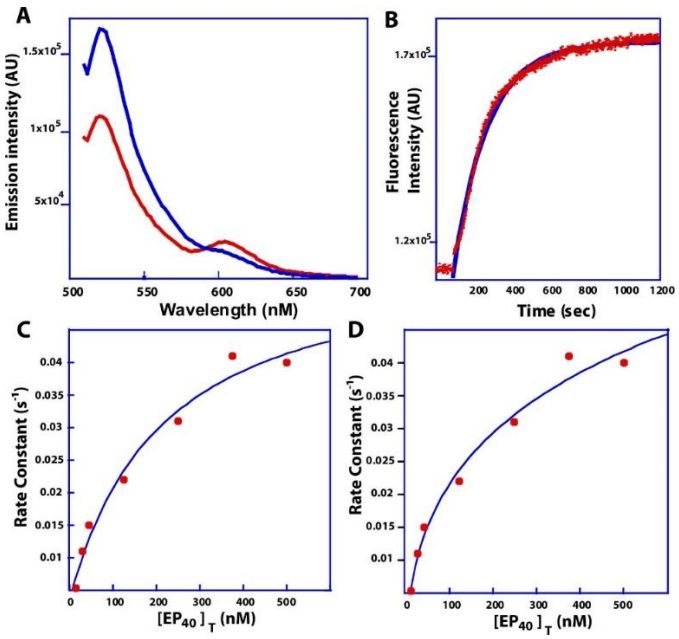

Figure 5. Data Set 5 analysis. A. Before (blue) and after (red) fluorescence emission scans (excitation=498 nm) of 10 nM Flo-18M-1-Rox with SgrAI in the presence of 10 mM $MgCl_2$. The peak at 520 nm corresponds to the Flo emission maximum, and the emission at 605 nm corresponds to that of Rox. Before reaction (and DNA cleavage) by SgrAI, a strong Rox signal is seen largely due to FRET from Flo (a small amount of Rox emission derives from Rox absorbance at 498 nm). After reaction with SgrAI (and DNA cleavage and strand separation) the Flo emission increases due to reduced FRET to Rox resulting in reduced Rox emission. AU, arbitrary units. **B.** Fluorescence emission data at 520 nm with excitation at 498 nm (red filled circles) of a Data Set 5 reaction of 10 nM Flo-18M-1-Rox, excess SgrAI, and in the presence of 10 mM $MgCl_2$. AU, arbitrary units. Data after 100 sec are fit to a single exponential function (blue line) giving a rate constant of $5x10^{-3}\pm4x10^{-5}$ s^{-1}, and R=0.996. **C.** Analytically derived rate constants for Data Set 5 vs. total EP_{40} concentration (SgrAI bound to self-annealed PC DNA) shown as red filled circles. Hill analysis (blue line) with Hill coefficient forced to 1 gives a $K_{1/2}$ of 0.2±0.1 µM, and R=0.990 and an upper asymptote of $5.8\pm0.9x10^{-2}$ s^{-1}. **D.** Hill plot with fitted Hill coefficient. $K_{1/2}$=2±50 µM, N=0.4±1, R=0.991.

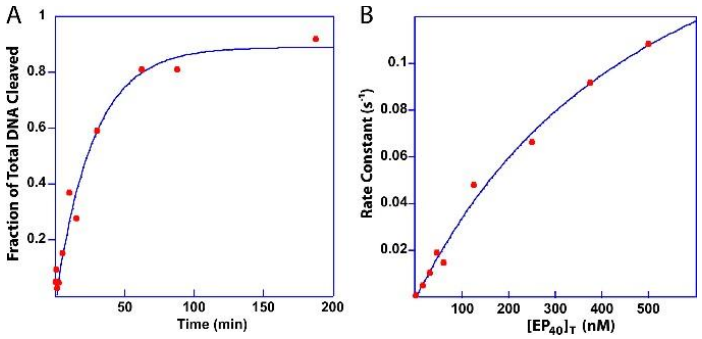

Figure 6. Data Set 7 analysis. A. Example of analytical data fitting from densitometric scan data. Data (red circles) were fit to a single exponential function (blue line) to give a rate constant (see Experimental Procedures). The fit gives 0.037 min^{-1} for the rate constant, with R=0.984. **B.** Hill Plot of Data Set 7 single exponential rate constants, plotted vs. the total concentration of EP_{40} (SgrAI bound to self-annealed PC DNA). $K_{1/2}$=0.5±0.5 µM, and Hill coefficient N=1.0±0.3, upper asymptote, 0.22±0.12 s^{-1}, and R=0.995.

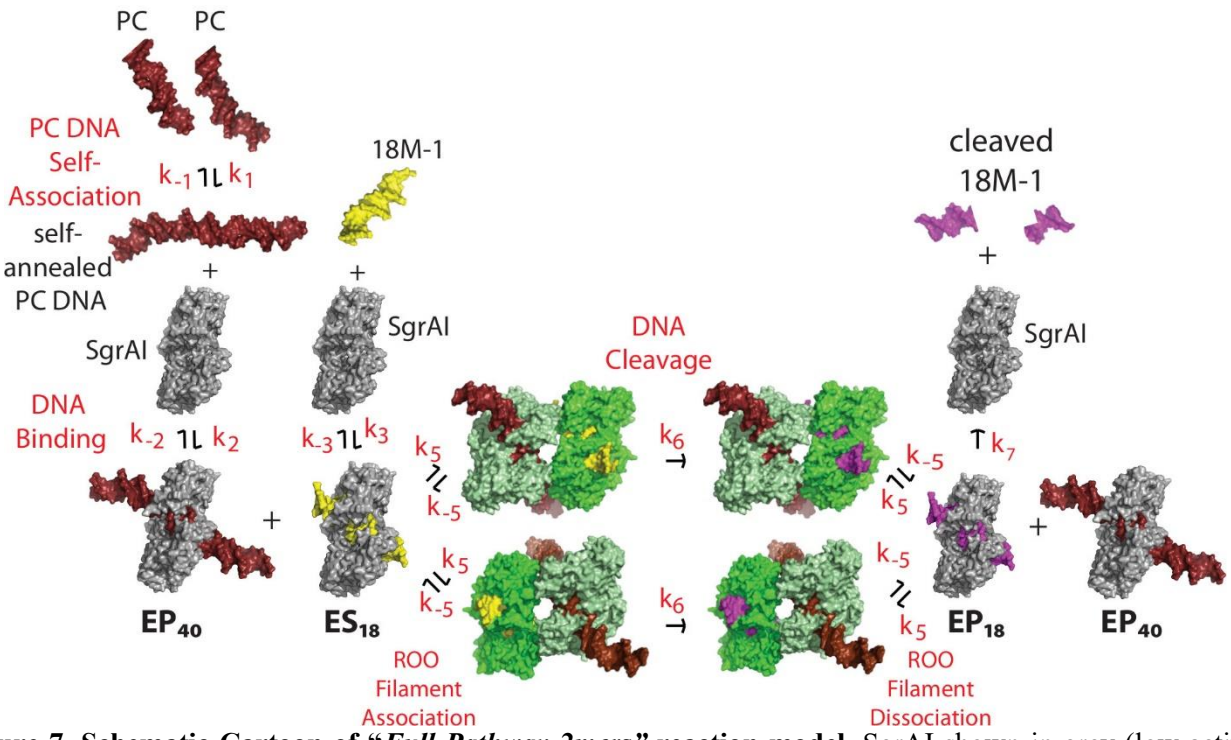

Figure 7. Schematic Cartoon of "*Full Pathway 2mers*" reaction model. SgrAI shown in grey (low activity conformation) or green (high activity conformation) and DNA shown in brown for PC DNA, and yellow or purple for uncleaved or cleaved 18M-1 DNA, respectively. Numbered rate constants are shown and correspond to the forward and reverse rate constants (see also **Table S8**) for: association of two PC DNA molecules to a semi-continuous 40mer (k_1, k_{-1}), binding of SgrAI to self-annealed PC DNA to create EP_{40} (k_2, k_{-2}), binding of SgrAI to 18M-1 DNA to create ES_{18} (k_3, k_{-3}), association of ES_{18} with EP_{40} (two orientations for association are possible)(k_5, k_{-5}), **c**leavage of 18M-1 DNA (although both top and bot strands are cleaved independently, only a single cleavage event is shown for simplicity) in ES_{18} to create EP_{18} (k_6)**, d**issociation of EP_{40} from EP_{18}, for simplicity, these rate constants are set to be identical for the association and dissociation of EP_{40} and ES_{18} (k_5, k_{-5}), dissociation of EP_{18} into SgrAI and cleaved 18M-1 (k_{-3}, considered equivalent to dissociation of uncleaved 18M-1 DNA from SgrAI). Cleaved 18M-1 dissociates into single strands and is considered irreversible (not shown).

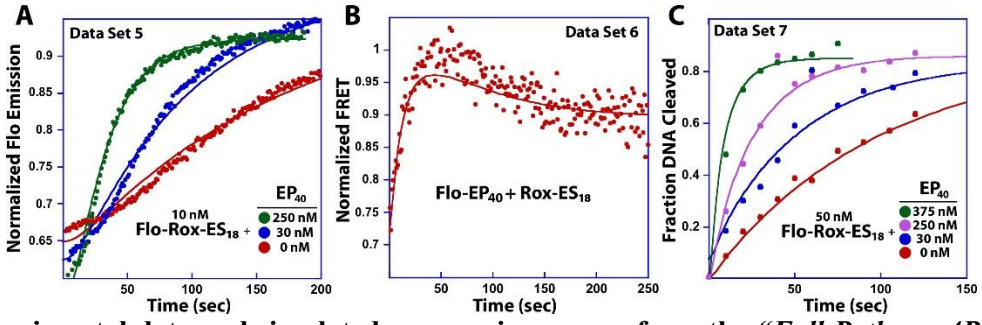

Figure 8. Experimental data and simulated progression curves from the *"Full Pathway 4BM"* model. **A.** Experimental data (filled circles) and simulated signals (lines) from select reactions of Data Set 5. Starting concentrations of Flo-ES_{18}-Rox (SgrAI bound to Flo-18M-1-Rox) and EP_{40} (SgrAI bound to self-annealed PC DNA) as shown. **B.** Experimental data (filled circles) and simulated signal (line) for a reaction from Data Set 6. **C.** Experimental data (filled circles) and simulated signals (lines) from select reactions of Data Set 7. Starting concentrations of Flo-ES_{18}-Rox (SgrAI bound to Flo-18M-1-Rox) and EP_{40} (SgrAI bound to self-annealed PC DNA) as shown.

Supporting Information
for

The run-on oligomer filament enzyme mechanism of SgrAI.
Part 2: Kinetic Modeling of the full DNA cleavage pathway

Chad K. Park, Jonathan L. Sanchez, Claudia Barahona, L. Emilia Basantes, Juan Sanchez, Christian Hernandez, and N. C. Horton

From the Department of Molecular and Cellular Biology, University of Arizona, Tucson, AZ 85721

Results

DNA binding by SgrAI

Because DNA binding is part of the kinetic pathways modeled in this work, the forward and reverse rate constants for this initial substrate binding reaction were estimated. SgrAI binds to DNA containing its recognition sequences in a 1:1 complex of SgrAI dimer:duplex DNA, and DNA binding by SgrAI is assumed to be rapid and diffusion limited, hence an estimate of 10^9 M^{-1} s^{-1} was used for the forward association rate constant, k_F. This estimate of the forward rate constant then allows the reverse rate constant to be calculated from the measured K_D ($K_D=k_R/k_F$). The DNA sequences used in this study include "18M-1", an 18 bp DNA duplex with a single primary recognition sequence, and PC DNA, where each PC DNA is one-half of a "pre-cleaved" 40 bp DNA containing a single primary recognition sequence (see Experimental Procedures). The shorter DNA, 18M-1, was designed to dissociate irreversibly upon cleavage in both strands. On the other hand, PC DNA self-anneals into Pre-Cleaved Double Stranded or PCDS, which binds SgrAI and stimulates fun-on oligomer (ROO) filament formation (and activation of DNA cleavage).

Previously, the K_D of SgrAI binding to a version of 18M-1 called "18-1" where the base pairs flanking the SgrAI recognition sequence differ slightly, (see Experimental Procedures and below for sequences) was previously measured in the presence of divalent cation (Ca^{2+} as a proxy for Mg^{2+}) and found to be 0.6±0.2 nM (1). However, some reactions in the present work were performed without divalent cations. Therefore, fluorescence polarization anisotropy measurements were performed with Hex (6-(4,7,2',4',5',7'-Hexachloro-3',6'-dipivaloylfluoresceinyl)) labeled 18-1 DNA and SgrAI to determine the K_D without divalent cations, giving a K_D of 11±2 nM. This K_D was used as a constraint during global data fitting of the ratio of the reverse to the forward rate constants for DNA binding. For binding of SgrAI to PC DNA, the K_D in the absence and presence of divalent cations was assumed to be the same as that measured for 40-1 (2.3 nM and 0.06 nM, respectively) a DNA nearly identical to self-annealed PC DNA (2). Importantly, these rate constants did not affect or limit the modeling significantly, since processes following DNA binding are rate limiting in the reactions studied here.

Investigation of cooperativity using simulations

Next, to test if the mere formation of ROO filaments can give rise to cooperativity in simulated data, simulations of the type of titration data shown in **Fig. 2**, namely the FRET signal from Rox-ES_{18} with increasing concentrations of initial or total Flo-EP_{40}, were prepared. These used the equations for ROO filament assembly found in the ***"Filament Assembly 5EO"*** model (blue, **Fig. S8**), but because the association rate constants appear to depend on the presence of divalent cations (being approximately tenfold slower in the presence of either 10 mM $CaCl_2$ or 10 mM $MgCl_2$, see Part 1 (2) and this work, respectively), rate constants from the ***"Full Pathway 4BM"*** model which fitted reaction data containing 10 mM $MgCl_2$ were also used (red lines, **Fig. S8**). First, the percentage of ES_{18} found in ROO filaments was simulated as a function of total EP_{40} (**Fig. S8A**). A fit of the data to the Hill equation resulted in Hill coefficients of 1.03±0.01 nM and 0.98±0.01 nM, depending on the rate constants used (**Fig. S8A**), indicating no evidence of cooperativity by this measure. Next, this exercise was repeated but with the predicted FRET signal (**Fig. S8B**), and again, a fit to the Hill equation showed no cooperativity. Since the ***"Filament Assembly 5EO"*** model only includes ROO filaments up to only 5 SgrAI/DNA complexes, but simulations from Part 1 (2) indicate that larger ROO filaments form significantly at concentrations

of EP_{40} above 250 nM, additional equations allowing ROO filaments up to 9 SgrAI/DNA complexes were added to a modified version of the ***"Filament Assembly 5EO"*** model (**Table S15-S16**). Using this model, the data were simulated then fit and again a Hill coefficient N of 1 was found, indicating no cooperativity on total [EP_{40}], and with a $K_{1/2}$ of 230 nM and 1200 nM, depending on which rate constants were used (**Fig. S8C**). Interestingly, when the experimental data are fit to a Hill equation with N forced to 1, the $K_{1/2}$ is also 1200 nM (**Fig. S7**).

Experimental Procedures

DNA used in binding affinity measurements

18-1-top **5'-AAGTCCA|CCGGTGGACTT-3'**

The DNA sequence is self-complementary, hence anneals to form the 18bp duplex 18-1.

Fluorescence Polarization Assay for DNA binding by SgrAI

Fluorescence polarization anisotropy was used to investigate the binding affinities of SgrAI to Hex labeled 18-1 DNA in 1.5 ml buffer A, by titrating with increasing concentrations of SgrAI. Fluorescence anisotropy was measured using excitation at 537 nm (Hex) in a PC1 (ISS) fluorometer with T format, automatic polarizers at 25°C. The emitted intensities were measured using a 50.8 mm diameter 570 nm cut-on filter with a 580-2750 nm transmittance range (ThermoOriel Inc., catalog no. 59510) and 1 mm (8 nm) slit widths. The resulting data were fit using the following equation (8):

$$A = A_{min} + (A_{max} - A_{min}) \times \frac{\{P_T + O_T + K_D - [(P_T + O_T + K_D)^2 - (4 \times P_T \times O_T)^{1/2}]\}}{2 \times O_T}$$

Where A is the anisotropy for the current concentration of added SgrAI, A_{max} and A_{min} are the maximum and minimum anisotropy values corresponding to that for no and full binding of the DNA, respectively. P_T, O_T, and K_D correspond to the total amount of SgrAI (protein), DNA (oligonucleotide, 10 nM), and equilibrium dissociation constant, respectively.

Global data fitting

Data from Data Set 5 were fit to the following type of equation:

$$Experimentally\ measured\ Flo\ Intensity\ at\ time\ t = baseline + (scaling\ factor) \times (simulated\ concentration\ of\ cleaved\ and\ released\ Flo - 18M - 1 - Rox\ at\ time\ t)$$

The Flo emission unquenches when separated from Rox, following cleavage and dissociation of the double stranded and doubly labeled Flo-18M-1-Rox (**Fig. 2B**). Because the stability of the duplex form of cleaved 18-1 is so weak, it is expected to dissociate irreversibly to single strands, and therefore dissociation from SgrAI is considered irreversible after release of cleaved Flo-18M-1-Rox. The baselines and scaling factors were fit independently for each data set in each model (see below).

Data Set 7 data also utilizes Flo-18-1-Rox, however it analyzes the products by denaturing PAGE to separate the cleaved strands. Quantitation of these products was done using fluorescence imaging and densitometry of the gels following electrophoresis. The quantitated cleaved and uncleaved DNA was used to calculate a fraction of the total DNA cleaved for both top (Rox labeled) and bottom (Rox labeled) strands. The data were fit to equations of the form:

$$Experimentally\ measured\ percentage\ of\ cleaved\ top\ or\ bottom\ strands\ at\ time\ t = baseline + (scaling\ factor) \times (Total\ simulated\ cleaved\ DNA\ at\ time\ t)$$

The experimentally measured percentage of cleaved top or bottom strands of DNA at time t was determined using denaturing PAGE and therefore includes all cleaved DNA, regardless of whether it was bound to SgrAI at the time of quenching or not, and therefore simulations of this quantity include cleaved DNA bound to SgrAI (see below for equations used). The baselines and scaling factors were fit independently for each data set in each model.

Data from reactions containing Rox-18M-1 and Flo-PC and no $MgCl_2$ (Data Set 4) were fit separately from the other data sets to determine forward and reverse rate constants for the association of SgrAI/Rox-18M-1 with SgrAI/Flo-PC in isolation from subsequent reaction steps. These reactions are limited to the initial equilibria between DNA binding and association of SgrAI/DNA complexes due to the absence of Mg^{2+} (DNA cleavage does not occur).

Fitting predicted concentrations of species to the actual data required scaling factors which was straight forward for Data Set 5 and 7 data as described above. However, for the FRET data of Data Sets 4 and 6, the degree of FRET between fluorophores in oligomers must be predicted, which will depend on their relative separation in the oligomer. This was done as described in Part 1 (2), and software specific equations are given below.

Predicted progression curves were fit to the normalized data using estimated or fitted rate constants, and baseline and scaling factors fit for each experiment. All attempts were made to limit the number of fitted parameters.

Figures and Tables

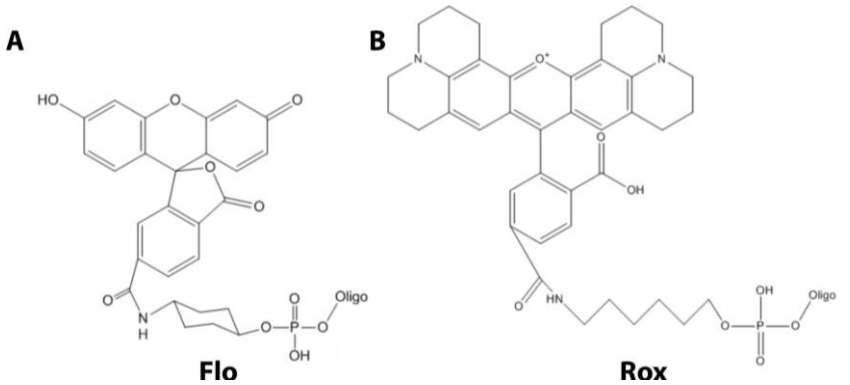

Figure S1. Chemical structure diagrams of fluorophores and their linkage chemistry used in kinetic studies. A. Flo or 6-carboxyfluorescein, connected to the 5'phosphate of the DNA strand via a trans-4-cyclohexanol linker. **B.** Rox or 5(6)-carboxy-X-rhodamine, connected to the 5'phosphate of the DNA strand via a 6-amino hexan-1-ol linker.

Table S1. Experimental variables, including starting concentrations, in each reaction

Data Set	Reaction ID	[SgrAI]	[18M-1] (nM) and type[a]	[PC DNA] (nM) and type[b]	[Mg^{2+}] (mM)	Order of Mixing	Rate Constant from Analytical Fitting (s^{-1})
4	251	200	50 (Rox)	90 (Flo)	0	adding SgrAI last	ND[c]
	252	250	50 (Rox)	120 (Flo)	0	adding SgrAI last	ND[c]
	253	250	50 (Rox)	150 (Flo)	0	adding SgrAI last	ND[c]
	254	150	50 (Rox)	50 (Flo)	0	adding SgrAI last	ND[c]
	255	250	100 (Rox)	100 (Flo)	0	adding SgrAI last	ND[c]
	256	250	150 (Rox)	50 (Flo)	0	adding SgrAI last	ND[c]
5	101	50	10 (Flo-Rox)	30 (Unl)	10	adding SgrAI last	0.0053
	102	100	10 (Flo-Rox)	60 (Unl)	10	adding SgrAI last	0.011
	103	100	10 (Flo-Rox)	90 (Unl)	10	adding SgrAI last	0.015
	105	300	10 (Flo-Rox)	250 (Unl)	10	adding SgrAI last	0.022
	106	300	10 (Flo-Rox)	500 (Unl)	10	adding SgrAI last	0.031

	107	500	10 (Flo-Rox)	750 (Unl)	10	adding SgrAI last	0.041
	108	600	10 (Flo-Rox)	1000 (Unl)	10	adding SgrAI last	0.040
6	201	200	100 (Rox)	100 (Flo)	10	adding Rox-18M-1 last	ND[c]
	202	350	200 (Rox)	200 (Flo)	10	adding Rox-18M-1 last	ND[c]
	203	150	50 (Rox)	50 (Flo)	10	adding Rox-18M-1 last	ND[c]
	204	150	50 (Rox)	25 (Flo)	10	adding Rox-18M-1 last	ND[c]
	205	200	50 (Rox)	150 (Flo)	10	adding Rox-18M-1 last	ND[c]
	206	150	50 (Rox)	100 (Flo)	10	adding Rox-18M-1 last	ND[c]
7	401	1000	50 (Flo-Rox)	0 (Unl)	10	adding SgrAI last	$5.5x10^{-4}$
	402	1000	50 (Flo-Rox)	30 (Unl)	10	adding SgrAI last	$5.1x10^{-3}$
	403	1000	50 (Flo-Rox)	60 (Unl)	10	adding SgrAI last	0.0105
	404	1000	50 (Flo-Rox)	90 (Unl)	10	adding SgrAI last	0.0189
	405	1000	50 (Flo-Rox)	120 (Unl)	10	adding SgrAI last	0.0146
	406	1000	50 (Flo-Rox)	250 (Unl)	10	adding SgrAI last	0.0480
	407	1000	50 (Flo-Rox)	500 (Unl)	10	adding SgrAI last	0.0662
	408	1000	50 (Flo-Rox)	750 (Unl)	10	adding SgrAI last	0.0918
	409	1000	50 (Flo-Rox)	1000 (Unl)	10	adding SgrAI last	0.109

[a]Rox, 5' Rox top strand only labeled DNA, Flo-Rox, 5'Rox top strand and 5'Flo bot strand labeled DNA.
[b]Flo, 5'Flo top strand labeled DNA, Unl, unlabeled DNA.
[c]ND, not determined.

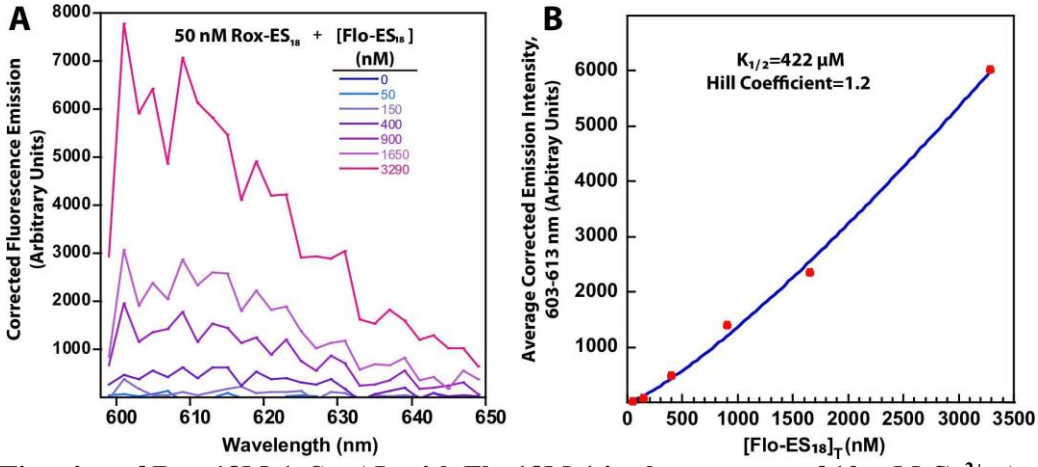

Figure S2. Titration of Rox-18M-1, SgrAI, with Flo-18M-1 in the presence of 10 mM Ca^{2+}. A. 50 nM Rox-18M-1, 2 µM SgrAI (4 µM SgrAI for highest concentration of Flo-18M-1), 10 mM $CaCl_2$, and buffer A (see Experimental Procedures) with Flo-18M-1 (1:4 Flo-18M-1:18M-1) at 25°C. Emission spectra taken with 498 nm excitation, and corrected for Flo emission (using a scaled emission from 1 µM PC DNA (1:9 Flo-PC:PC DNA) with 1 µM SgrAI at 25°C and in buffer A with 10 mM $CaCl_2$, scaling factor calculated from relative emissions at 570 nm), dilution, and Rox emission due to absorption at 498 nm (using the emission collected before adding Flo-PC). **B.** Average corrected intensities from A (wavelengths 602-612 nm) vs. added $[Flo\text{-}ES_{18}]_T$ (the concentration of SgrAI bound to Flo-18M-1, with Flo-18M-1 being composed of 1:4 Flo-18M-1:18M-1)(closed blue circles). Fit to Hill plot (red line) gives $K_{1/2}$=422 µM and Hill coefficient=1.2, however curve is poorly determined due to weak binding.

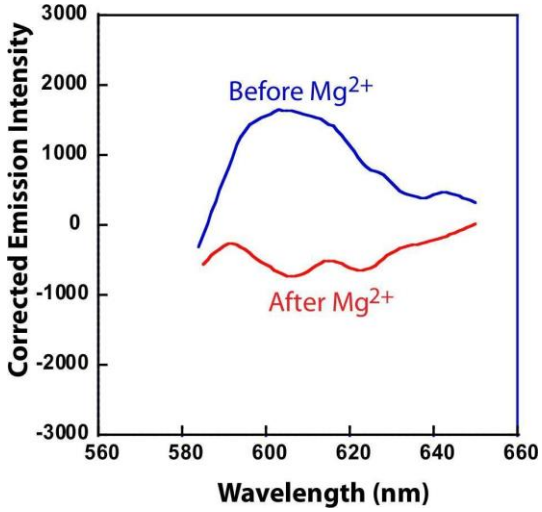

Figure S3. Test for residual FRET and trapping of Rox-18M-1. Blue line: 2 µM SgrAI, 2 µM Flo-PC, 200 nM Rox-18M-1, Red line: after (15 minutes) addition of 10 mM $MgCl_2$ at 25°C. Emission spectra taken with 498 nm excitation, and corrected for Flo emission (using a scaled emission from 1 µM PC DNA (1:9 Flo-PC:PC DNA), scaling factor calculated from relative emissions at 584-586 nm), dilution, and Rox emission due to absorption at 498 nm (using the emission collected before adding Flo-PC but after addition of SgrAI). A slight negative peak appears in the red trace due to the additional quenching of Rox by the presence of Mg^{2+}.

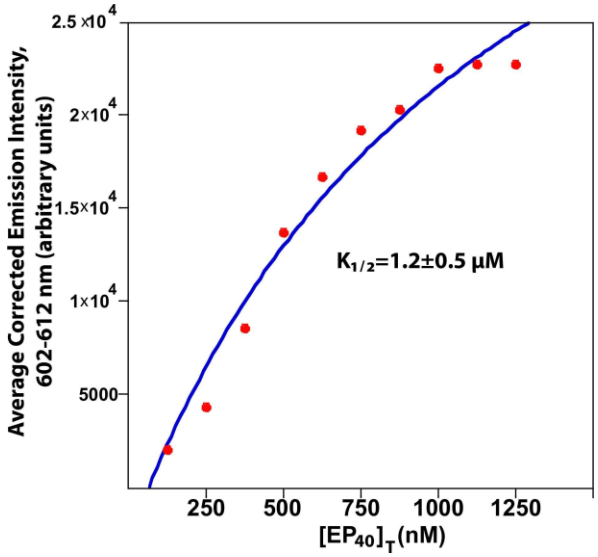

Figure S4. Titration of Rox-18M-1, SgrAI, with Flo-PC DNA in the presence of 10 mM Ca^{2+}. Fit to Hill equation with N, the Hill coefficient, forced to equal 1. $[EP_{40}]_T$ is the total concentration of SgrAI bound to two copies of PC DNA (equal to the concentration of added PC DNA divided by 2). $K_{1/2}$=1.2±0.5 µM.

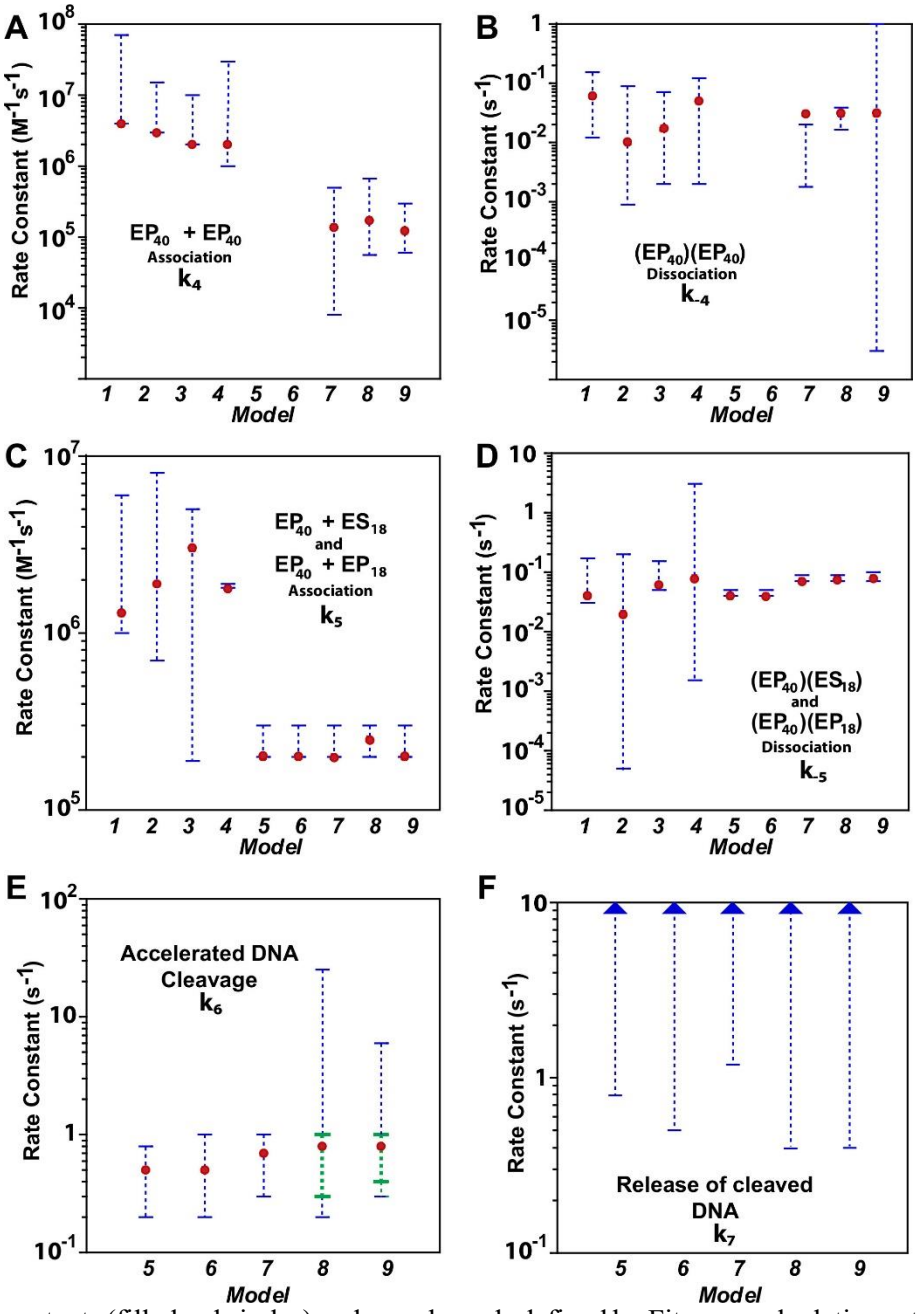

Figure S5. Rate constants (filled red circles) and error bounds defined by Fitspace calculations at 0.95 χ^2 threshold (blue bars and dashed lines) for the different models (1 = ***"Filament Assembly 5EO"***, 2 = ***"Filament Assembly 5BM",*** 3 = ***"Filament Assembly 4EO",*** 4 = ***"Filament Assembly 4BM"***, 5 = ***"Full Pathway 2mers Independent Strand Cleavage"***, 6 = ***"Full Pathway 2mers"***, 7 = ***"Full Pathway 3mers",*** 8 = ***"Full Pathway 4EO",*** 9 = ***"Full Pathway 4BM").*** Green bars and dashed lines indicate error bounds at 0.99 χ^2 threshold. **A.** Association rate constant for EP_{40} with EP_{40}, k_4. **B.** Dissociation rate constant of two associated EP_{40}, k_{-4}. **C.** Association rate constants for ES_{18} (or EP_{18}) with EP_{40}, k_5. **D.** Dissociation rate constant of a complex between ES_{18} (or EP_{18}) and EP_{40}, k_{-5}. **E.** Accelerated DNA cleavage rate constant within an ROO (*i.e.* by ES_{18} associated with at least one EP_{40}), k_6. **F.** Rate constant for release of cleaved DNA from EP_{18}, k_7. Only the lower boundary is given as no upper boundary is defined by the data.

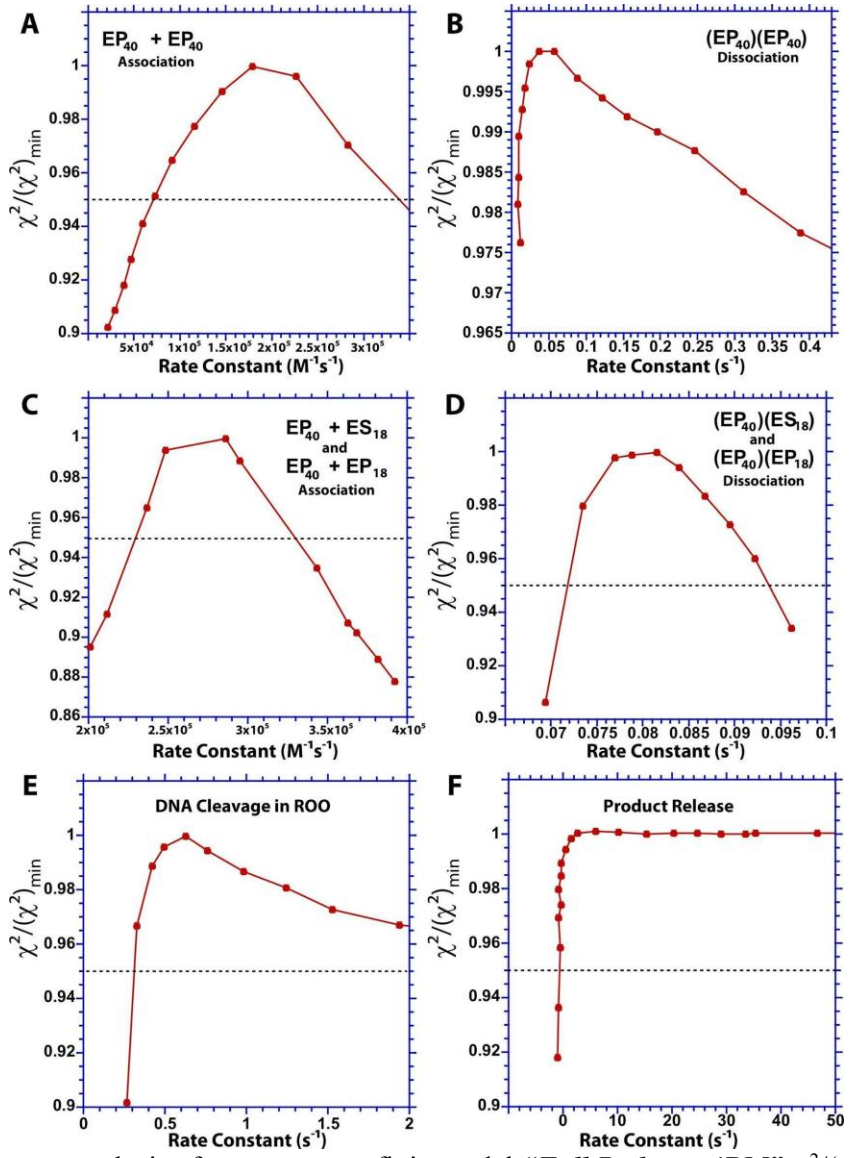

Figure S6. Fitspace error analysis of rate constants fit in model ***"Full Pathway 4BM"***. $\chi^2/(\chi^2)_{min}$ is a measure of the goodness of fit of the model to the experimental data, with a value of 1 giving the best fit. **A.** Association rate constant for two SgrAI complexes both bound to self-annealed PC DNA (EP_{40}). **B.** Dissociation rate constant of two associated EP_{40}. **C.** Association rate constant for two SgrAI complexes, one bound to 18M-1 (ES_{18} or EP_{18}, when DNA is uncleaved or cleaved, respectively) and one bound to self-annealed PC DNA (EP_{40}). **D.** Dissociation rate constant of associated EP_{40} and ES_{18} (or EP_{18}). **E.** Accelerated DNA cleavage rate constant when ES_{18} is bound to EP_{40}. **F.** Dissociation rate constant for dissociation of cleaved 18M-1 from EP_{18}. The dotted line indicates a $\chi^2/(\chi^2)_{min}$ of 0.95.

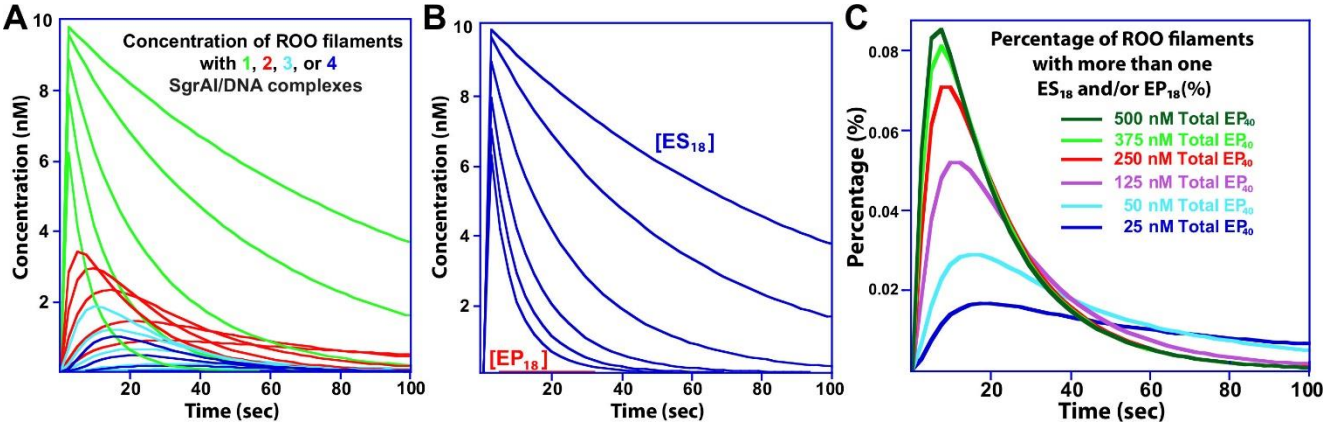

Figure S7. Concentration of SgrAI/DNA in run-on oligomers of different sizes during the DNA cleavage reaction using the model *"Full Pathway 4BM"*. **A**. Run-on oligomers having 1 (red), 2 (green), 3 (blue), or 4 (yellow) SgrAI/DNA complexes (with at least 1 ES_{18} or EP_{18}) were scaled for the number of SgrAI bound to 18M-1 DNA (ES_{18} and/or EP_{18}) and presented in concentration units (nM). Starting concentrations were 10 nM 18M-1, 1 μM SgrAI, and a range of total EP_{40} (SgrAI bound to self-annealed PC DNA) concentrations: 25, 50, 125, 250, 375, 500 nM. **B**. As in A, with concentrations of ES_{18} (SgrAI bound to uncleaved 18M-1) shown in the pink line, and EP_{18} (SgrAI bound to cleaved 18M-1) in the light blue line. **C.** Percentage of species containing more than one ES_{18} (SgrAI bound to Flo-18M-1-Rox) in the ***"Full Pathway 4BM"*** model with 1 μM SgrAI, 10 nM Flo-18M-1-Rox, and varied total EP_{40}.

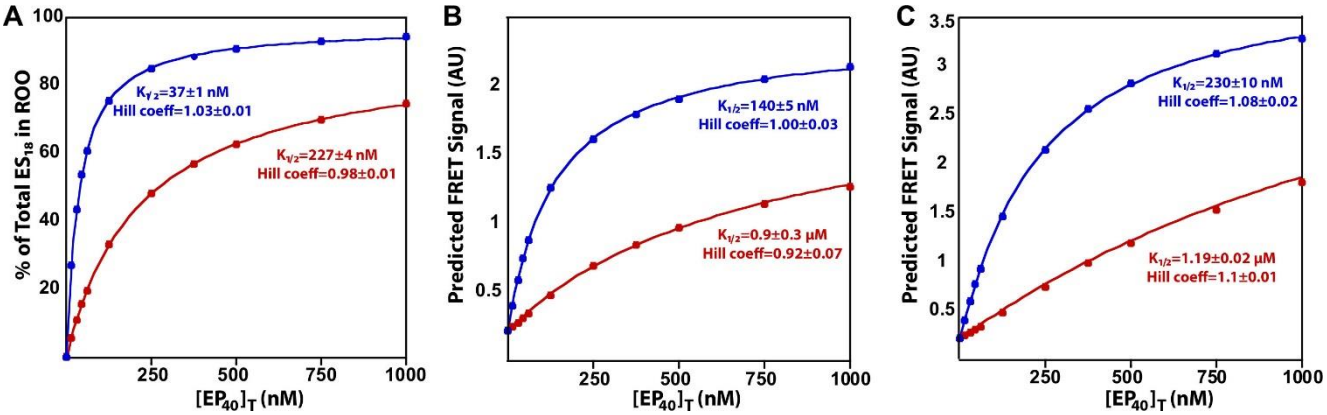

Figure S8. Predicted percentage of SgrAI/DNA complexes in ROO filaments and FRET signal as a function of total [EP_{40}] (*i.e.* SgrAI bound to PC DNA). A. Percentage of total ES_{18} to be in a ROO filament of at least 2 SgrAI/DNA complexes as a function of total EP_{40} concentration (all forms including in ROO filaments), using rate constants from either ***"Filament Assembly 5EO"*** (blue) or ***"Full Pathway 4BM"*** (red) models. Fits of the simulated data to the Hill equation gives $K_{1/2}$ and Hill coefficients shown, with R=0.9996 and 0.9999 for blue and red lines, respectively). Initial concentrations of 18M-1 and SgrAI were 50 nM and 4 μM, respectively. **B.** Predicted normalized FRET signal. Rate constants and colors as in A. Scaling factors in both plots from the ***"Filament Assembly 5EO"*** model (baseline=0.2111, scaling factor=0.05606, a=0.2, b=0.12, c=0.96), and starting concentrations of 18M-1 and SgrAI are 50 nM and 4 μM, respectively. Quality of fits are R=0.99986 and 0.99969 for the blue and red lines, respectively. AU, arbitrary units. **C.** Predicted normalized FRET signal as a function of [PC] using the ***"Filament Assembly 5EO"*** model modified to allow ROO filaments up to 9 SgrAI/DNA complexes. Colors as in A, and scaling factors as in B. Quality of fits was R=0.99994 and 0.99876 for the blue and red lines, respectively. AU, arbitrary units.

Table S2. Parameters for *"Full Pathway 4BM"* fitting with increasing positive cooperativity

Cooperativity Factor	Sigma with respect to the fit	χ^2 [a]	χ^2/DoF[b]
1	0.021	6073	1.8
2	0.020	6129	1.8
5	0.021	7772	2.3
10	0.023	10382	3.1

[a]χ^2 or Chi^2 is the sum of the squares of the residuals between each experimental data point and its simulated value. [b]DoF is Degrees of Freedom, calculated from the number of data points N and number of fitted parameters. Values of χ^2/DoF closer to 1 indicate better fits.

Kintek Global Kinetic Explorer (3) Models

Equations for models to fit Data Set 4 reactions

Table S3. Equations describing equilibria modeled in *"Filament Assembly 5EO"* and *"Filament Assembly 4EO" models* (7 total independent rate constants, k_1, k_2, k_3, k_4, k_{-4}, k_5, k_{-5})

Self-association of PC DNA into A-DNA[a]		
Left-PC DNA + Right-PC-DNA ⇌ **A-DNA**	k_1	k_{-1} (constrained by calculated K_D of 376 µM and not fit independently)
SgrAI binding to self-annealed activating DNA (A-DNA) or Rox labeled reporter DNA (R-DNA) into SgrAI/DNA complexes A and R, respectively		
SgrAI+**A-DNA** ⇌ **A**	k_2	k_{-2} (constrained by measured K_D and not fit independently)[b]
SgrAI+**R-DNA** ⇌ **R**	k_3	k_{-3} (constrained by measured K_D and not fit independently)[c]
Self-assembly of SgrAI/DNA Complexes (SgrAI/A-DNA complex is denoted as A, SgrAI/R-DNA complex is denoted as R)		
*Self-associations where SgrAI/**A-DNA** (i.e. **A**) binds to another SgrAI/**A-DNA** (i.e. **A**) Both models*		
A + A ⇌ AA	k_4	k_{-4}
A + A ⇌ AA	k_4	k_{-4}
RA + A ⇌ RAA	k_4	k_{-4}
A + AR ⇌ AAR	k_4	k_{-4}
AA + A ⇌ AAA	k_4	k_{-4}
A + AA ⇌ AAA	k_4	k_{-4}
AAA + A ⇌ AAAA	k_4	k_{-4}
A + AAA ⇌ AAAA	k_4	k_{-4}
A + AAR ⇌ AAAR	k_4	k_{-4}
ARA + A ⇌ ARAA	k_4	k_{-4}
RAA + A ⇌ RAAA	k_4	k_{-4}
***"Filament Assembly 5EO"** only*		
A + AAAA ⇌ AAAAA	k_4	k_{-4}

AAAA + A ⇌ AAAAA	k_4	k_{-4}
A + AAAR ⇌ AAAAR	k_4	k_{-4}
A + AARA ⇌ AAARA	k_4	k_{-4}
A + ARAA ⇌ AARAA	k_4	k_{-4}
AARA + A ⇌ AARAA	k_4	k_{-4}
ARAA + A ⇌ ARAAA	k_4	k_{-4}
RAAA + A ⇌ RAAAA	k_4	k_{-4}
A + ARAR ⇌ AARAR	k_4	k_{-4}
RARA + A ⇌ RARAA	k_4	k_{-4}
*Associations where SgrAI/**R-DNA** (i.e. **R**) binds to a SgrAI/**A-DNA** (i.e. **A**)* *Both models*		
A + R ⇌ AR	k_5	k_{-5}
R + A ⇌ RA	k_5	k_{-5}
A + RA ⇌ ARA	k_5	k_{-5}
AR + A ⇌ ARA	k_5	k_{-5}
R + AR ⇌ RAR	k_5	k_{-5}
RA + R ⇌ RAR	k_5	k_{-5}
AAR + A ⇌ AARA	k_5	k_{-5}
R + AAR ⇌ RAAR	k_5	k_{-5}
RAR + A ⇌ RARA	k_5	k_{-5}
A + RAR ⇌ ARAR	k_5	k_{-5}
AAA + R ⇌ AAAR	k_5	k_{-5}
A + RAA ⇌ ARAA	k_5	k_{-5}
R + AAA ⇌ RAAA	k_5	k_{-5}
*Associations where SgrAI/**R-DNA** (i.e. **R**) binds to a SgrAI/**A-DNA** (i.e. **A**)* ***"Filament Assembly 5EO"** only*		
AAAA + R ⇌ AAAAR	k_5	k_{-5}
AAAR + A ⇌ AAARA	k_5	k_{-5}
A + RAAA ⇌ ARAAA	k_5	k_{-5}
R + AAAA ⇌ RAAAA	k_5	k_{-5}
AARA + R ⇌ AARAR	k_5	k_{-5}
A + RARA ⇌ ARARA	k_5	k_{-5}
ARAR + A ⇌ ARARA	k_5	k_{-5}
R + ARAA ⇌ RARAA	k_5	k_{-5}
A + RAAR ⇌ ARAAR	k_5	k_{-5}
ARAA + R ⇌ ARAAR	k_5	k_{-5}
R + AARA ⇌ RAARA	k_5	k_{-5}
R + AAAR ⇌ RAAAR	k_5	k_{-5}
RAAA + R ⇌ RAAAR	k_5	k_{-5}
R + ARAR ⇌ RARAR	k_5	k_{-5}
RARA + R ⇌ RARAR	k_5	k_{-5}

[a]A value of 376 μM was used for the K_D of this equilibrium (2).

[b]A value of 2.3 nM was used for the K_D, which is was measured for SgrAI and a Flo-40-1 DNA (since self-annealed PC DNA mimics a cleaved version of the 40 bp DNA containing a single primary recognition site, 40-

1) (2).
[c]A value of 11 nM was used for the K_D of this equilibrium (see above, ***DNA binding by SgrAI*** section).

Table S4. Additional reactions to add to *"Filament Assembly 5EO"* and *"Filament Assembly 4EO"* to give *"Filament Assembly 5BM"* and *"Filament Assembly 4BM"*

Reaction Step	Forward Rate Constant	Reverse Rate Constant
Self-assembly of SgrAI/DNA Complexes (SgrAI/A-DNA complex is denoted as A, SgrAI/R-DNA complex is denoted as R)		
*Self-associations where SgrAI/**A-DNA** (i.e. A) binds to another SgrAI/**A-DNA** (i.e. A) Both models*		
AA+AA ⇌ AAAA	k_4	k_{-4}
AA+AR ⇌ AAAR	k_4	k_{-4}
RA+AA ⇌ RAAA	k_4	k_{-4}
RA+AR ⇌ RAAR	k_4	k_{-4}
***"Filament Assembly 5BM"** only*		
AA + AAA ⇌ AAAAA	k_4	k_{-4}
AAA + AA ⇌ AAAAA	k_4	k_{-4}
AA + AAR ⇌ AAAAR	k_4	k_{-4}
AAA + AR ⇌ AAAAR	k_4	k_{-4}
AA + ARA ⇌ AAARA	k_4	k_{-4}
RA + AAA ⇌ RAAAA	k_4	k_{-4}
RAA + AA ⇌ RAAAA	k_4	k_{-4}
ARA + AR ⇌ ARAAR	k_4	k_{-4}
RA + ARA ⇌ RAARA	k_4	k_{-4}
RA + AAR ⇌ RAAAR	k_4	k_{-4}
RAA + AR ⇌ RAAAR	k_4	k_{-4}
*Associations where SgrAI/**R-DNA** (i.e. R) binds to a SgrAI/**A-DNA** (i.e. A) Both models*		
AA+RA ⇌ AARA	k_5	k_{-5}
AR+AA ⇌ ARAA	k_5	k_{-5}
AA+RR ⇌ AARR	k_5	k_{-5}
RR+AA ⇌ RRAA	k_5	k_{-5}
RA+RA ⇌ RARA	k_5	k_{-5}
AR+AR ⇌ ARAR	k_5	k_{-5}
RR+AR ⇌ RRAR	k_5	k_{-5}
RA+RR ⇌ RARR	k_5	k_{-5}
***"Filament Assembly 5BM"** only*		
AAA + RA ⇌ AAARA	k_5	k_{-5}
AA + RAA ⇌ AARAA	k_5	k_{-5}
AAR + AA ⇌ AARAA	k_5	k_{-5}
AR + AAA ⇌ ARAAA	k_5	k_{-5}
AAR + AA ⇌ ARAAA	k_5	k_{-5}
AA + RAR ⇌ AARAR	k_5	k_{-5}
AR + ARA ⇌ ARARA	k_5	k_{-5}

ARA + RA ⇌ ARARA	k_5	k_{-5}
RA + RAA ⇌ RARAA	k_5	k_{-5}
RAR + AA ⇌ RARAA	k_5	k_{-5}
AR + AAR ⇌ ARAAR	k_5	k_{-5}
RAA + RA ⇌ RAARA	k_5	k_{-5}
RA + RAR ⇌ RARAR	k_5	k_{-5}
RAR + AR ⇌ RARAR	k_5	k_{-5}

Table S5. Equation for data fitting in *"Filament Assembly"* models (2 fitted constants per reaction (baseline and scaling factor), and six reactions to fit, gives 12 total fitted constants)

Data Fitted	Equation or Explanation
FRET signal from Flo labeled SgrAI/A-DNA complexes (A) and Rox labeled SgrAI/R-DNA complexes (R) in the larger filamentous assembly	Simulated FRET signal = Baseline correction factor + Scaling factor × (Sum of weighted concentration of all FRET pair complexes)
Baseline correction factor (individually fit for each reaction)	This is used to simulate the fluorescence signal observed prior to the reaction, which is nonzero due to non-FRET processes (such as emission from the donor Flo, or emission from the acceptor Rox due to absorption at the excitation wavelength)
Scaling factor (individually fit for each reaction)	This scales the fluorescence signal to the normalized predicted signal based on concentrations of individual distinct assemblies of A and R.
a, b, c (held constant for all reactions)	These are weighting factors for the predicted efficiency of the FRET signal from a given donor (A) and acceptor (R) pair based on their orientation in the filamentous assembly predicted using the molecular model derived from cryo-electron microscopy (see (2)). a=0.2, b=0.12, c=0.96
Sum of weighted concentration of all FRET pair complexes (dependent on simulated concentrations, as determined by rate constants and starting concentrations)	a[AR]+a[RA]+(a+b)[AAR]+2a[ARA]+(a+c)[RAA]+(2a+b)[AARA]+(a+b+c)[AAAR]+(2a+b)[ARAA]+(a+b+c)[RAAA]+(a+b+c)[AAAAR]+(2a+b+c)[AAARA]+(2a+2b)[AARAA]+(2a+b+c)[ARAAA]+(a+b+c)[RAAAA]+(2a)[RAR]+(2a+2b)[RAAR]+(a+c)[RARA]+(3a+c)[ARAR]+(3a+b+c)[AARAR]+(4a+2c)[ARARA]+(3a+b+c)[RARAA]+(3a+2b)[ARAAR]+(3a+2b)[RAARA]+(2a+2b+2c)[RAAAR] +(4a+2c)[RARAR])

Models for fitting the full DNA cleavage pathway using combined Data Sets 5-7

Table S6. Equations for the "*Full Pathway 2mers Independent Strand Cleavage" model* (with a total of 8 independent rate constants k_1, k_2, k_3, k_5, k_{-5}, k_6, k_7, k_8)

Reaction Step	Forward Rate Constant	Reverse Rate Constant
Self-association of PC DNA into A-DNA		
Left-PC DNA + Right-PC-DNA ⇌ **A-DNA**	k_1	k_{-1} (constrained by calculated K_D of 376 μM and not fit independently)[a]
SgrAI binding to self-annealed activating DNA (A-DNA) or Rox labeled reporter DNA (R-DNA) into SgrAI/DNA complexes A and R, respectively		
SgrAI+**A-DNA** ⇌ **A**	k_2	k_{-2} (constrained by measured K_D and not fit independently)[b]
SgrAI+**R-DNA** ⇌ **R**	k_3	k_{-3} (constrained by measured K_D and not fit independently)[c]
Association of a SgrAI/A-DNA complex (i.e. A) with a SgrAI/R-DNA complex (i.e. R)		
A + **R** ⇌ **AR**	k_5	k_{-5}
R + **A** ⇌ **RA**	k_5	k_{-5}
Cleavage of DNA within the ROO filament (R becomes X^T or X^B, for cleavage of top or bot strands, respectively, then X^{TB} for cleavage in both strands)		
AR ⇌ **A**X^T	k_6	set to zero, to make DNA cleavage irreversible
RA ⇌ X^T**A**	k_6	set to zero, to make DNA cleavage irreversible
AR ⇌ **A**X^B	k_6	set to zero, to make DNA cleavage irreversible
RA ⇌ X^B**A**	k_6	set to zero, to make DNA cleavage irreversible
AX^T ⇌ **A**X^{TB}	k_6	set to zero, to make DNA cleavage irreversible
X^T**A** ⇌ X^{TB}**A**	k_6	set to zero, to make DNA cleavage irreversible
AX^B ⇌ **A**X^{TB}	k_6	set to zero, to make DNA cleavage irreversible
X^B**A** ⇌ X^{TB}**A**	k_6	set to zero, to make DNA cleavage irreversible
Dissociation of SgrAI/R-DNA complex containing cleaved reporter DNA (i.e. X^{TB}) from a SgrAI/A-DNA complex (i.e. A) (the same rate constants are assumed here as above, with SgrAI bound to uncleaved R-DNA)		
AX^T ⇌ **A** + X^T	k_{-5}	k_5
X^T**A** ⇌ X^T + **A**	k_{-5}	k_5
AX^B ⇌ **A** + X^B	k_{-5}	k_5
X^B**A** ⇌ X^B + **A**	k_{-5}	k_5
AX^{TB} ⇌ **A** + X^{TB}	k_{-5}	k_5
X^{TB}**A** ⇌ X^{TB} + **A**	k_{-5}	k_5
Dissociation of cleaved reporter DNA (R-DNA^{cleaved}) from SgrAI (the same rate constants are assumed here as above, for binding to uncleaved R-DNA)		

$X^{TB} \rightleftharpoons$ SgrAI + R-DNA^{cleaved}	k_7	set to zero to make this step irreversible
DNA cleavage of reporter DNA by SgrAI not in a ROO filament		
$R \rightleftharpoons X^{T}$	k_8	set to zero to make this step irreversible
$R \rightleftharpoons X^{B}$	k_8	set to zero to make this step irreversible
$X^{T} \rightleftharpoons X^{TB}$	k_8	set to zero to make this step irreversible
$X^{B} \rightleftharpoons X^{TB}$	k_8	set to zero to make this step irreversible

Table S7. Equations used in fitting the *"Full Pathway 2mers Independent Cleavage"* model (with a total of 50 different fitted constants)

Type of Data	Equation[a]	Number of fitted parameters
Data Set 5, FRET from donor labeled activator (Flo-PC or A-DNA when self-annealed) and acceptor labeled reporter (Rox-18M-1 or R-DNA) when associated into a ROO filament (baseline correction factor and scaling factors 1-2 were fit separately for each reaction)[a]	simulated signal=baseline correction factor +(scaling factor 1) × ([AR]+[RA]+[AX^{T}]+[AX^{B}]+ [A X^{TB}]+[X^{T}A]+[X^{B}A]+]+[X^{TB}A]) + (scaling factor 2)[R-DNA^{cleavedtop}]	6 reactions with 3 constants (baseline and 2 scaling factors) = 18
Data Set 6, Gain of Flo signal due to loss of FRET from doubly labeled reporter DNA (Flo-18M-1-Rox or R-DNA) lost upon release of cleaved reporter DNA from SgrAI (baseline correction factor and scaling factor were fit separately for each reaction)	simulated signal=baseline correction factor + (scaling factor) × [R-DNA^{cleavedbot}]	7 reactions with 2 constants (baseline and scaling factor) = 14
Data Set 7, Fraction or Percent of doubly labeled reporter DNA (Flo-18M-1-Rox or R-DNA) that is cleaved, whether bound to SgrAI or not (baseline correction factor and scaling factor were fit separately for each reaction)[b]	simulated signal=baseline correction factor +(scaling factor) × ([R-DNA^{cleaved}]+ [R-DNA^{cleaved}]+ [X^{TB}]+ [X^{B}]+[AX^{TB}]+2[AX^{B}]+[X^{TB}A]+ [X^{B}A])	9 reactions with 2 constants (baseline and scaling factor) = 18

[a]Some emission from the Rox labeled bottom strand persists even after DNA cleavage and separation from the donor, due to absorbance of the Rox dye at the excitation wavelength of 498 nm.

[b]The two strands of the reporter R-DNA, Flo-18M-1-bot and Rox-18M-1-top, are resolved in the urea-PAGE and quantified separately, and the equation shown as written is relevant to the signal from the bot (Flo) strand. However, this equation is also applicable to the top (Rox) strand as well, since cleavage of both strands is modeled as concurrent, and dissociation of cleaved DNA leads to equal concentrations of top and bot strands. Since the baseline and scaling factors are different for the Flo and Rox quantification in the urea-PAGE gel, the reactions with each strand were quantitated and subsequently fit separately for each in each reaction.

Table S8. Equations for simulating the reaction pathway in the *"Full Pathway 2mers"* model (with a total of 8 independent rate constants k_1, k_2, k_3, k_5, k_{-5}, k_6, k_7, k_8)

Reaction Step	Forward Rate Constant	Reverse Rate Constant
Self-association of PC DNA into A-DNA		
Left-PC DNA + Right-PC-DNA ⇌ A-DNA	k_1	k_{-1} (constrained by calculated K_D of 376 µM and not fit independently)[a]
SgrAI binding to self-annealed activating DNA (A-DNA) or Rox labeled reporter DNA (R-DNA) into SgrAI/DNA complexes A and R, respectively		

SgrAI+**A-DNA** ⇌ **A**	k_2	k_{-2} (constrained by measured K_D and not fit independently)[b]
SgrAI+**R-DNA** ⇌ **R**	k_3	k_{-3} (constrained by measured K_D and not fit independently)[c]
Association of a SgrAI/A-DNA complex (i.e. A) with a SgrAI/R-DNA complex (i.e. R)		
A + **R** ⇌ **AR**	k_4	k_{-4}
R + **A** ⇌ **RA**	k_4	k_{-4}
Cleavage of DNA within the ROO filament (R becomes X)		
AR ⇌ **AX**	k_6	set to zero, to make DNA cleavage irreversible
RA ⇌ **XA**	k_6	set to zero, to make DNA cleavage irreversible
Dissociation of SgrAI/R-DNA complex with cleaved reporter DNA (i.e. X) from a SgrAI/A-DNA complex (i.e. A) (the same rate constants are assumed here as above, with SgrAI bound to uncleaved R-DNA)		
AX ⇌ **A** + **X**	k_{-4}	k_4
XA ⇌ **X** + **A**	k_{-4}	k_4
Dissociation of cleaved reporter DNA from SgrAI (the same rate constants are assumed here as above, for binding to uncleaved R-DNA)		
X ⇌ SgrAI + **R-DNA**$^{\textbf{cleaved}}$	k_7	set to zero, to make DNA cleavage irreversible
DNA cleavage of reporter DNA by SgrAI not in a ROO filament		
R ⇌ **X**	k_8	set to zero, to make DNA cleavage irreversible

Table S9. Equations used in simulating and fitting reaction data to the "*Full Pathway 2mers*" model (with a total of 50 fitted constants)

Type of Data	Equation	Number of fitted parameters
Data Set 5, FRET from donor labeled activator (Flo-PC or **A-DNA** when self-annealed) and acceptor labeled reporter (Rox-18M-1 or **R-DNA**) when associated into a ROO filament (baseline correction factor and scaling factors 1-3 were fit separately for each reaction)[a]	simulated signal=baseline correction factor+(scaling factor 1) × ([**AR**]+[**RA**]+[**AX**]+[**XA**]+ (scaling factor 3)[**R-DNA**$^{\textbf{cleaved}}$]	6 reactions with 3 constants (baseline and 2 scaling factors) = 18
Data Set 6, gain of Flo signal due to loss of FRET from doubly labeled reporter DNA (Flo-18M-1-Rox or **R-DNA**) lost upon release of cleaved reporter DNA from SgrAI (baseline correction factor and scaling factor were fit separately for each reaction)	simulated signal=baseline correction factor + (scaling factor) × [**R-DNA**$^{\textbf{cleaved}}$]	7 reactions with 2 constants (baseline and scaling factor) = 14
Data Set 7, Fraction or Percent of doubly labeled reporter DNA (Flo-18M-1-Rox or **R-DNA**) that is cleaved, whether bound to SgrAI or not (baseline correction factor and scaling factor were fit separately for each reaction)[b]	simulated signal=baseline correction factor +(scaling factor) × ([**R-DNA**$^{\textbf{cleaved}}$]+[**X**]+[**AX**]+[**XA**])	9 reactions with 2 constants (baseline and scaling factor) = 18

[a]Some emission from the Rox labeled bottom strand persists even after DNA cleavage and separation from the donor, due to absorbance of the Rox dye at the excitation wavelength of 498 nm.

[b]The two strands of the reporter **R-DNA**, Flo-18M-1-bot and Rox-18M-1-top, are resolved in the urea-PAGE and quantified separately, and the equation shown as written is relevant to the signal from the bot (Flo) strand. However, this equation is also applicable to the top (Rox) strand as well, since cleavage of both strands is modeled as concurrent, and dissociation of cleaved DNA leads to equal concentrations of top and bot strands. Since the baseline and scaling factors are different for the Flo and Rox quantification in the urea-PAGE gel, the reactions with each strand were quantitated and subsequently fit separately for each in each reaction.

Table S10. Equations for simulating the reaction pathway in the "*Full Pathway 3mers*" model (with a total of 10 independent rate constants k_1, k_2, k_3, k_4, k_{-5}, k_5, k_{-5}, k_6, k_7, k_8)

Reaction Step	Forward Rate Constant	Reverse Rate Constant
Self-association of PC DNA into A-DNA		
Left-PC DNA + Right-PC-DNA ⇌ **A-DNA**	k_1	k_{-1} (constrained by calculated K_D of 376 μM and not fit independently)[a]
SgrAI binding to self-annealed activating DNA (A-DNA) or Rox labeled reporter DNA (R-DNA) into SgrAI/DNA complexes A and R, respectively		
SgrAI+**A-DNA** ⇌ **A**	k_2	k_{-2} (constrained by measured K_D and not fit independently)[b]
SgrAI+**R-DNA** ⇌ **R**	k_3	k_{-3} (constrained by measured K_D and not fit independently)[c]
Self-association of a SgrAI/A-DNA complex (i.e. A) with another SgrAI/A-DNA complex (i.e. A)		
A + **A** ⇌ **AA**	k_4	k_{-4}
A + **A** ⇌ **AA**	k_4	k_{-4}
RA + **A** ⇌ **RAA**	k_4	k_{-4}
A + **AR** ⇌ **AAR**	k_4	k_{-4}
AA + **A** ⇌ **AAA**	k_4	k_{-4}
A + **AA** ⇌ **AAA**	k_4	k_{-4}
Association of a SgrAI/A-DNA complex (i.e. A) with a SgrAI/R-DNA complex (i.e. R)		
A + **R** ⇌ **AR**	k_5	k_{-5}
R + **A** ⇌ **RA**	k_5	k_{-5}
AR + **A** ⇌ **ARA**	k_5	k_{-5}
A + **RA** ⇌ **ARA**	k_5	k_{-5}
AA + **R** ⇌ **AAR**	k_5	k_{-5}
R + **AA** ⇌ **RAA**	k_5	k_{-5}
R + **AR** ⇌ **RAR**	k_5	k_{-5}
RA + **R** ⇌ **RAR**	k_5	k_{-5}
Cleavage of DNA within the ROO filament (R becomes X)		
AR ⇌ **AX**	k_6	set to zero, to make DNA cleavage irreversible
RA ⇌ **XA**	k_6	set to zero, to make DNA cleavage irreversible
ARA ⇌ **AXA**	k_6	set to zero, to make DNA cleavage irreversible
AAR ⇌ **AAX**	k_6	set to zero, to make DNA cleavage irreversible
RAA ⇌ **XAA**	k_6	set to zero, to make DNA cleavage irreversible
RAR ⇌ **XAR**	k_6	set to zero, to make DNA cleavage irreversible
RAR ⇌ **RAX**	k_6	set to zero, to make DNA cleavage irreversible
XAR ⇌ **XAX**	k_6	set to zero, to make DNA cleavage irreversible
RAX ⇌ **XAX**	k_6	set to zero, to make DNA cleavage

		irreversible
Association of a SgrAI/A-DNA complex (i.e. A) with another SgrAI/A-DNA complex (i.e. A)		
AA ⇌ **A** + **A**	k_{-4}	k_4
AA ⇌ **A** + **A**	k_{-4}	k_4
XAA ⇌ **XA** + **A**	k_{-4}	k_4
AAX ⇌ **A** + **AX**	k_{-4}	k_4
AAA ⇌ **AA** + **A**	k_{-4}	k_4
AAA ⇌ **A** + **AA**	k_{-4}	k_4
Dissociation of SgrAI/R-DNA complex with cleaved reporter DNA (i.e. X) from a SgrAI/A-DNA complex (i.e. A) (the same rate constants are assumed here as above, with SgrAI bound to uncleaved R-DNA)		
AX ⇌ **A** + **X**	k_{-5}	k_5
RA ⇌ **X** + **A**	k_{-5}	k_5
AXA ⇌ **AX** + **A**	k_{-5}	k_5
AXA ⇌ **A** + **XA**	k_{-5}	k_5
AAX ⇌ **AA** + **X**	k_{-5}	k_5
XAA ⇌ **X** + **AA**	k_{-5}	k_5
XAR ⇌ **X** + **AR**	k_{-5}	k_5
XAR ⇌ **XA** + **R**	k_{-5}	k_5
RAX ⇌ **R** + **AX**	k_{-5}	k_5
RAX ⇌ **RA** + **X**	k_{-5}	k_5
XAX ⇌ **X** + **AX**	k_{-5}	k_5
XAX ⇌ **XA** + **X**	k_{-5}	k_5
Dissociation of cleaved reporter DNA from SgrAI (the same rate constants are assumed here as above, for binding to uncleaved R-DNA)		
X ⇌ SgrAI + **R-DNA**^{cleaved}	k_7	set to zero, to make DNA cleavage irreversible
DNA cleavage of reporter DNA by SgrAI not in a ROO filament		
R ⇌ **X**	k_8	set to zero, to make DNA cleavage irreversible

Table S11. Equations used in simulating and fitting reaction data to the "*Full Pathway 3mers*" model (with a total of 50 fitted constants)

Type of Data	Equation	Number of fitted parameters
Data Set 5, FRET from donor labeled activator (Flo-PC or **A-DNA** when self-annealed) and acceptor labeled reporter (Rox-18M-1 or **R-DNA**) when associated into a ROO filament (baseline correction factor and scaling factors 1-3 were fit separately for each reaction)[a]	simulated signal=baseline correction factor+(scaling factor 1)×([**AR**]+[**RA**]+[**RAA**]+[**ARA**]+[**AAR**]+2[**RAR**]+[**AX**]+[**XA**]+[**XAA**]+[**AXA**]+[**AAX**]+2[**XAX**]+2[**RAX**]+2[**XAR**])(scaling factor 2)[**R-DNA**^{cleaved}]	6 reactions with 3 constants (baseline and 2 scaling factors) = 18
Data Set 6, Gain of Flo emission due to loss of FRET from doubly labeled reporter DNA (Flo-18M-1-Rox or **R-DNA**) lost upon release of cleaved reporter DNA from SgrAI (baseline correction factor and scaling factor were fit separately for each reaction)	simulated signal=baseline correction factor + (scaling factor)[**R-DNA**^{cleaved}]	7 reactions with 2 constants (baseline and scaling factor) = 14

Data Set 7, Fraction or Percent of doubly labeled reporter DNA (Flo-18M-1-Rox or **R-DNA**) that is cleaved, whether bound to SgrAI or not (baseline correction factor and scaling factor were fit separately for each reaction)[b]	simulated signal=baseline correction factor + (scaling factor) ([**R-DNA**^{cleaved}] +[**X**]+[**AX**]+[**XA**]+[**XAA**]+[**AXA**]+[**AAX**]+2[**XAX**]+ [**RAX**]+[**XAR**])	9 reactions with 2 constants (baseline and scaling factor) = 18

[a]Some emission from the Rox labeled bottom strand persists even after DNA cleavage and separation from the donor, due to absorbance of the Rox dye at the excitation wavelength of 498 nm.
[b]The two strands of the reporter **R-DNA**, Flo-18M-1-bot and Rox-18M-1-top, are resolved in the urea-PAGE and quantified separately, and the equation shown as written is relevant to the signal from the bot (Flo) strand. However, this equation is also applicable to the top (Rox) strand as well, since cleavage of both strands is modeled as concurrent, and dissociation of cleaved DNA leads to equal concentrations of top and bot strands. Since the baseline and scaling factors are different for the Flo and Rox quantification in the urea-PAGE gel, the reactions with each strand were quantitated and subsequently fit separately for each in each reaction.

Table S12. Equations for simulating the reaction pathway in the model "*Full Pathway 4EO*" (with a total of 10 independent rate constants k_1, k_2, k_3, k_4, k_{-5}, k_5, k_{-5}, k_6, k_7, k_8)

Reaction Step	Forward Rate Constant	Reverse Rate Constant
Self-association of PC DNA into A-DNA		
Left-PC DNA + Right-PC-DNA ⇌ **A-DNA**	k_1	k_{-1} (constrained by calculated K_D of 376 µM and not fit independently)[a]
SgrAI binding to self-annealed activating DNA (A-DNA) or Rox labeled reporter DNA (R-DNA) into SgrAI/DNA complexes A and R, respectively		
SgrAI+**A-DNA** ⇌ **A**	k_2	k_{-2} (constrained by measured K_D and not fit independently)[b]
SgrAI+**R-DNA** ⇌ **R**	k_3	k_{-3} (constrained by measured K_D and not fit independently)[c]
Self-association of a SgrAI/A-DNA complex (i.e. A) with another SgrAI/A-DNA complex (i.e. A)		
A + **A** ⇌ **AA**	k_4	k_{-4}
A + **A** ⇌ **AA**	k_4	k_{-4}
RA + **A** ⇌ **RAA**	k_4	k_{-4}
A + **AR** ⇌ **AAR**	k_4	k_{-4}
AA + **A** ⇌ **AAA**	k_4	k_{-4}
A + **AA** ⇌ **AAA**	k_4	k_{-4}
AAA + **A** ⇌ **AAAA**	k_4	k_{-4}
A + **AAA** ⇌ **AAAA**	k_4	k_{-4}
A + **AAR** ⇌ **AAAR**	k_4	k_{-4}
A + **ARA** ⇌ **AARA**	k_4	k_{-4}
ARA + **A** ⇌ **ARAA**	k_4	k_{-4}
RAA + **A** ⇌ **RAAA**	k_4	k_{-4}
Association of a SgrAI/A-DNA complex (i.e. A) with a SgrAI/R-DNA complex (i.e. R)		
A + **R** ⇌ **AR**	k_5	k_{-5}
R + **A** ⇌ **RA**	k_5	k_{-5}
AR + **A** ⇌ **ARA**	k_5	k_{-5}
A + **RA** ⇌ **ARA**	k_5	k_{-5}
AA + **R** ⇌ **AAR**	k_5	k_{-5}
R + **AA** ⇌ **RAA**	k_5	k_{-5}

R + AR ⇌ RAR	k_5	k_{-5}
RA + R ⇌ RAR	k_5	k_{-5}
R + AAA ⇌ RAAA	k_5	k_{-5}
R + AAR ⇌ RAAR	k_5	k_{-5}
RAA + R ⇌ RAAR	k_5	k_{-5}
R + ARA ⇌ RARA	k_5	k_{-5}
RAR + A ⇌ RARA	k_5	k_{-5}
A + RAR ⇌ ARAR	k_5	k_{-5}
ARA + R ⇌ ARAR	k_5	k_{-5}
AAA + R ⇌ AAAR	k_5	k_{-5}
AAR + A ⇌ AARA	k_5	k_{-5}
A + RAA ⇌ ARAA	k_5	k_{-5}
Cleavage of DNA within the ROO filament (R becomes X)		
AR ⇌ AX	k_6	set to zero, to make DNA cleavage irreversible
RA ⇌ XA	k_6	set to zero, to make DNA cleavage irreversible
ARA ⇌ AXA	k_6	set to zero, to make DNA cleavage irreversible
AAR ⇌ AAX	k_6	set to zero, to make DNA cleavage irreversible
RAA ⇌ XAA	k_6	set to zero, to make DNA cleavage irreversible
RAR ⇌ XAR	k_6	set to zero, to make DNA cleavage irreversible
RAR ⇌ RAX	k_6	set to zero, to make DNA cleavage irreversible
XAR ⇌ XAX	k_6	set to zero, to make DNA cleavage irreversible
RAX ⇌ XAX	k_6	set to zero, to make DNA cleavage irreversible
AAAR ⇌ AAAX	k_6	set to zero, to make DNA cleavage irreversible
AARA ⇌ AAXA	k_6	set to zero, to make DNA cleavage irreversible
ARAA ⇌ AXAA	k_6	set to zero, to make DNA cleavage irreversible
RAAA ⇌ XAAA	k_6	set to zero, to make DNA cleavage irreversible
ARAR ⇌ ARAX	k_6	set to zero, to make DNA cleavage irreversible
ARAR ⇌ AXAR	k_6	set to zero, to make DNA cleavage irreversible
AXAR ⇌ AXAX	k_6	set to zero, to make DNA cleavage irreversible
ARAX ⇌ AXAX	k_6	set to zero, to make DNA cleavage irreversible
RAAR ⇌ RAAX	k_6	set to zero, to make DNA

		cleavage irreversible
RAAR ⇌ XAAR	k_6	set to zero, to make DNA cleavage irreversible
XAAR ⇌ XAAX	k_6	set to zero, to make DNA cleavage irreversible
RAAX ⇌ XAAX	k_6	set to zero, to make DNA cleavage irreversible
RARA ⇌ XARA	k_6	set to zero, to make DNA cleavage irreversible
RARA ⇌ RAXA	k_6	set to zero, to make DNA cleavage irreversible
XARA ⇌ XAXA	k_6	set to zero, to make DNA cleavage irreversible
XAXA ⇌ XAXA	k_6	set to zero, to make DNA cleavage irreversible
Self-association of a SgrAI/A-DNA complex (i.e. A) with another SgrAI/A-DNA complex (i.e. A)		
AA ⇌ A + A	k_{-4}	k_4
AA ⇌ A + A	k_{-4}	k_4
XAA ⇌ XA + A	k_{-4}	k_4
AAX ⇌ A + AX	k_{-4}	k_4
AAA ⇌ AA + A	k_{-4}	k_4
AAA ⇌ A + AA	k_{-4}	k_4
AAAX ⇌ A + AAX	k_{-4}	k_4
AAXA ⇌ A + AXA	k_{-4}	k_4
AXAA ⇌ AXA + A	k_{-4}	k_4
XAAA ⇌ XAA + A	k_{-4}	k_4
Dissociation of SgrAI/R-DNA complex with cleaved reporter DNA (i.e. X) from a SgrAI/A-DNA complex (i.e. A) (the same rate constants are assumed here as above, with SgrAI bound to uncleaved R-DNA)		
AX ⇌ A + X	k_{-5}	k_5
RA ⇌ X + A	k_{-5}	k_5
AXA ⇌ AX + A	k_{-5}	k_5
AXA ⇌ A + XA	k_{-5}	k_5
AAX ⇌ AA + X	k_{-5}	k_5
XAA ⇌ X + AA	k_{-5}	k_5
XAR ⇌ X + AR	k_{-5}	k_5
XAR ⇌ XA + R	k_{-5}	k_5
RAX ⇌ R + AX	k_{-5}	k_5
RAX ⇌ RA + X	k_{-5}	k_5
XAX ⇌ X + AX	k_{-5}	k_5
XAX ⇌ XA + X	k_{-5}	k_5
AAAX⇌ AAA + X	k_{-5}	k_5
AAXA ⇌ AAX + A	k_{-5}	k_5
AXAA ⇌ A + XAA	k_{-5}	k_5
XAAA ⇌ X + AAA	k_{-5}	k_5
AXAX ⇌ A + XAX	k_{-5}	k_5
AXAX ⇌ AXA + X	k_{-5}	k_5

XAAX ⇌ X + AAX	k_{-5}	k_5
XAAX ⇌ XAA + X	k_{-5}	k_5
XAXA ⇌ X + AXA	k_{-5}	k_5
XAXA ⇌ XAX + A	k_{-5}	k_5
ARAX ⇌ A + RAX	k_{-5}	k_5
ARAX ⇌ ARA + X	k_{-5}	k_5
AXAR ⇌ A + XAR	k_{-5}	k_5
AXAR ⇌ AXA + R	k_{-5}	k_5
RAAX ⇌ R + AAX	k_{-5}	k_5
RAAX ⇌ RAA + X	k_{-5}	k_5
XAAR ⇌ X + AAR	k_{-5}	k_5
XAAR ⇌ XAA + R	k_{-5}	k_5
RAXA ⇌ R + AXA	k_{-5}	k_5
RAXA ⇌ RAX + A	k_{-5}	k_5
XARA ⇌ X + ARA	k_{-5}	k_5
XARA ⇌ XAR + A	k_{-5}	k_5
Dissociation of cleaved reporter DNA from SgrAI (the same rate constants are assumed here as above, for binding to uncleaved R-DNA)		
X ⇌ SgrAI + R-DNA^{cleaved}	k_7	set to zero, to make DNA cleavage irreversible
DNA cleavage of reporter DNA by SgrAI not in a ROO filament		
R ⇌ X	k_8	k_{-8} (set to zero, to make DNA cleavage irreversible)

Table S13. Equations for simulating the reaction pathway in the model *"Full Pathway 4BM"* (with a total of 10 independent rate constants k_1, k_2, k_3, k_4, k_{-5}, k_5, k_{-5}, k_6, k_7, k_8)

Reaction Step	Forward Rate Constant	Reverse Rate Constant
Self-association of PC DNA into A-DNA		
Left-PC DNA + Right-PC-DNA ⇌ A-DNA	k_1	k_{-1} (constrained by calculated K_D of 376 μM and not fit independently)[a]
SgrAI binding to self-annealed activating DNA (A-DNA) or Rox labeled reporter DNA (R-DNA) into SgrAI/DNA complexes A and R, respectively		
SgrAI+A-DNA ⇌ A	k_2	k_{-2} (constrained by measured K_D and not fit independently)[b]
SgrAI+R-DNA ⇌ R	k_3	k_{-3} (constrained by measured K_D and not fit independently)[c]
Self-association of a SgrAI/A-DNA complex (i.e. A) with another SgrAI/A-DNA complex (i.e. A)		
A + A ⇌ AA	k_4	k_{-4}
A + A ⇌ AA	k_4	k_{-4}
RA + A ⇌ RAA	k_4	k_{-4}
A + AR ⇌ AAR	k_4	k_{-4}
AA + A ⇌ AAA	k_4	k_{-4}
A + AA ⇌ AAA	k_4	k_{-4}
AAA + A ⇌ AAAA	k_4	k_{-4}
A + AAA ⇌ AAAA	k_4	k_{-4}

A + AAR ⇌ AAAR	k_4	k_{-4}
A + ARA ⇌ AARA	k_4	k_{-4}
ARA + A ⇌ ARAA	k_4	k_{-4}
RAA + A ⇌ RAAA	k_4	k_{-4}
RA+AA ⇌ RAAA	k_4	k_{-4}
RA+AR ⇌ RAAR	k_4	k_{-4}
Association of a SgrAI/A-DNA complex (i.e. A) with a SgrAI/R-DNA complex (i.e. R)		
A + R ⇌ AR	k_5	k_{-5}
R + A ⇌ RA	k_5	k_{-5}
AR + A ⇌ ARA	k_5	k_{-5}
A + RA ⇌ ARA	k_5	k_{-5}
AA + R ⇌ AAR	k_5	k_{-5}
R + AA ⇌ RAA	k_5	k_{-5}
R + AR ⇌ RAR	k_5	k_{-5}
RA + R ⇌ RAR	k_5	k_{-5}
R + AAA ⇌ RAAA	k_5	k_{-5}
R + AAR ⇌ RAAR	k_5	k_{-5}
RAA + R ⇌ RAAR	k_5	k_{-5}
R + ARA ⇌ RARA	k_5	k_{-5}
RAR + A ⇌ RARA	k_5	k_{-5}
A + RAR ⇌ ARAR	k_5	k_{-5}
ARA + R ⇌ARAR	k_5	k_{-5}
AAA + R ⇌ AAAR	k_5	k_{-5}
AAR + A ⇌ AARA	k_5	k_{-5}
A + RAA ⇌ ARAA	k_5	k_{-5}
AA+RA ⇌ AARA	k_5	k_{-5}
AR+AA ⇌ ARAA	k_5	k_{-5}
AR+AR ⇌ ARAR	k_5	k_{-5}
RA+RA ⇌ RARA	k_5	k_{-5}
AA+AR ⇌ AAAR	k_5	k_{-5}
Cleavage of DNA within the ROO filament (R becomes X)		
AR ⇌ AX	k_6	k_{-6} (set to zero, to make DNA cleavage irreversible)
RA ⇌ XA	k_6	k_{-6} (set to zero, to make DNA cleavage irreversible)
ARA ⇌ AXA	k_6	k_{-6} (set to zero, to make DNA cleavage irreversible)
AAR ⇌ AAX	k_6	k_{-6} (set to zero, to make DNA cleavage irreversible)
RAA ⇌ XAA	k_6	k_{-6} (set to zero, to make DNA cleavage irreversible)
RAR ⇌ XAX	k_6	k_{-6} (set to zero, to make DNA cleavage irreversible)
AAAR ⇌ AAAX	k_6	k_{-6} (set to zero, to make DNA cleavage irreversible)

AARA ⇌ AAXA	k_6	k_{-6} (set to zero, to make DNA cleavage irreversible)
ARAA ⇌ AXAA	k_6	k_{-6} (set to zero, to make DNA cleavage irreversible)
RAAA ⇌ XAAA	k_6	k_{-6} (set to zero, to make DNA cleavage irreversible)
ARAR ⇌ ARAX	k_6	k_{-6} (set to zero, to make DNA cleavage irreversible)
ARAR ⇌ AXAR	k_6	k_{-6} (set to zero, to make DNA cleavage irreversible)
AXAR ⇌ AXAX	k_6	k_{-6} (set to zero, to make DNA cleavage irreversible)
ARAX ⇌ AXAX	k_6	k_{-6} (set to zero, to make DNA cleavage irreversible)
RAAR ⇌ XAAX	k_6	k_{-6} (set to zero, to make DNA cleavage irreversible)
RARA ⇌ XAXA	k_6	k_{-6} (set to zero, to make DNA cleavage irreversible)
Dissociation of a SgrAI/A-DNA complex (i.e. A) with another SgrAI/A-DNA complex (i.e. A)		
XAA ⇌ XA + A	k_{-4}	k_4
AAX ⇌ A + AX	k_{-4}	k_4
AAA ⇌ AA + A	k_{-4}	k_4
AAA ⇌ A + AA	k_{-4}	k_4
AAAX ⇌ A + AAX	k_{-4}	k_4
AAXA ⇌ A + AXA	k_{-4}	k_4
AXAA ⇌ AXA + A	k_{-4}	k_4
XAAA ⇌ XAA + A	k_{-4}	k_4
AAAA ⇌ AA+AA	k_{-4}	k_4
AAAX ⇌ AA+AX	k_{-4}	k_4
XAAA ⇌ XA+AA	k_{-4}	k_4
XAAX ⇌ XA+AX	k_{-4}	k_4
Dissociation of SgrAI/R-DNA complex with cleaved reporter DNA (i.e. X) from a SgrAI/A-DNA complex (i.e. A) (the same rate constants are assumed here as above, with SgrAI bound to uncleaved R-DNA)		
AX ⇌ A + X	k_{-5}	k_5
RA ⇌ X + A	k_{-5}	k_5
AXA ⇌ AX + A	k_{-5}	k_5
AXA ⇌ A + XA	k_{-5}	k_5
AAX ⇌ AA + X	k_{-5}	k_5
XAA ⇌ X + AA	k_{-5}	k_5
XAR ⇌ X + AR	k_{-5}	k_5
XAR ⇌ XA + R	k_{-5}	k_5
RAX ⇌ R + AX	k_{-5}	k_5
RAX ⇌ RA + X	k_{-5}	k_5
XAX ⇌ X + AX	k_{-5}	k_5
XAX ⇌ XA + X	k_{-5}	k_5
AAAX⇌ AAA + X	k_{-5}	k_5

AAXA ⇌ AAX + A	k_{-5}	k_5
AXAA ⇌ A + XAA	k_{-5}	k_5
XAAA ⇌ X + AAA	k_{-5}	k_5
AXAX ⇌ A + XAX	k_{-5}	k_5
AXAX ⇌ AXA + X	k_{-5}	k_5
XAAX ⇌ X + AAX	k_{-5}	k_5
XAAX ⇌ XAA + X	k_{-5}	k_5
XAXA ⇌ X + AXA	k_{-5}	k_5
XAXA ⇌ XAX + A	k_{-5}	k_5
ARAX ⇌ A + RAX	k_{-5}	k_5
ARAX ⇌ ARA + X	k_{-5}	k_5
AXAR ⇌ A + XAR	k_{-5}	k_5
AXAR ⇌ AXA + R	k_{-5}	k_5
RAAX ⇌ R + AAX	k_{-5}	k_5
RAAX ⇌ RAA + X	k_{-5}	k_5
XAAR ⇌ X + AAR	k_{-5}	k_5
XAAR ⇌ XAA + R	k_{-5}	k_5
RAXA ⇌ R + AXA	k_{-5}	k_5
RAXA ⇌ RAX + A	k_{-5}	k_5
XARA ⇌ X + ARA	k_{-5}	k_5
XARA ⇌ XAR + A	k_{-5}	k_5
AAXA ⇌ AA + XA	k_{-5}	k_5
AXAA ⇌ AX + AA	k_{-5}	k_5
AXAX ⇌ AX + AX	k_{-5}	k_5
XAXA ⇌ XA + XA	k_{-5}	k_5
Dissociation of cleaved reporter DNA from SgrAI (the same rate constants are assumed here as above, for binding to uncleaved R-DNA)		
X ⇌ SgrAI + R-DNA^{cleaved}	k_7	set to zero, to make DNA cleavage irreversible
DNA cleavage of reporter DNA by SgrAI not in a ROO filament		
R ⇌ X	k_8	k_{-8} (set to zero, to make DNA cleavage irreversible)

Table S14. Equations used in simulating and fitting reaction data to models *"Full Pathway 4EO"* and *"Full Pathway 4BM"* (with a total of 50 fitted constants each)

Type of Data	Equation	Number of fitted parameters
Data Set 5: FRET from donor labeled activator (Flo-PC or A-DNA when self-annealed) and acceptor labeled reporter (Rox-18M-1 or R-DNA) when associated into a ROO filament (baseline correction factor and scaling factors 1-2 were fit separately for each reaction)[a]	simulated signal = baseline correction factor + (scaling factor 1) × (a[FR]+a[RF]+(a+b)[FFR]+2a[FRF]+(a+c)[RFF]+(2a+b)[FFRF]+(a+b+c)[FFFR]+(2a+b)[FRFF]+(a+b+c)[RFFF]+(2a)[RFR]+(2a+2b)[RFFR]+(3a+c)[RFRF]+(3a+c)[FRFR]+a[FX]+a[XF]+(a+b)[FFX]+2a[FXF]+(a+c)[XFF]+(2a+b)[FFXF]+(a+b+c)[FFFX]+(2a+b)[FXFF]+(a+b+c)[XFFF]+(2a)[XFX]+(2a+2b)[XFFX]+(3a+c)[XFXF]+(3a+c)[FXFX]+(2a)[XFX]+(2a)[RFX]+(2a)[XFR]+(2a+2b)[XFFX]+(2a+2b)[RFFX]+	6 reactions with 3 constants (baseline and 2 scaling factors) = 18

	(2a+2b)[XFFR]+(3a+c)[XFXF]+(3a+c)[RFXF]+ (3a+c)[XFRF]+(3a+c)[FXFX]+(3a+c)[FRFX]+ (3a+c)[FRFX]) +(scaling factor 2)[R-DNA^{cleaved}]	
Data Set 6: gain of Flo signal due to loss of FRET from doubly labeled reporter DNA (Flo-18M-1-Rox or R-DNA) lost upon release of cleaved reporter DNA from SgrAI (baseline correction factor and scaling factor were fit separately for each reaction)	simulated signal=baseline correction factor + (scaling factor)[R-DNA^{cleaved}]	7 reactions with 2 constants (baseline and scaling factor) = 14
Data Set 7: Fraction or Percent of doubly labeled reporter DNA (Flo-18M-1-Rox or R-DNA) that is cleaved, whether bound to SgrAI or not (baseline correction factor and scaling factor were fit separately for each reaction)[b]	simulated signal=baseline correction factor + (scaling factor) × ([RDNA^{cleaved}]+[X]+[AX]+[XA]+[XAA]+[AXA]+[AAX]+2[XAX]+[RAX]+[XAR]+[AAAR]+[AARA]+[ARAA]+[RAAA]+[RARA]+[ARAR]+[AAAX]+[AAXA]+[AXAA]+[XAAA]+2[XAXA]+2[AXAX]+[RAXA]+[XARA]+[AXAR]+[ARAX])	9 reactions with 2 constants (baseline and scaling factor) = 18

[a]Some emission from the Rox labeled bottom strand persists even after DNA cleavage and separation from the donor, due to absorbance of the Rox dye at the excitation wavelength of 498 nm.

[b]The two strands of the reporter R-DNA, Flo-18M-1-bot and Rox-18M-1-top, are resolved in the urea-PAGE and quantified separately, and the equation shown as written is relevant to the signal from the bot (Flo) strand. However, this equation is also applicable to the top (Rox) strand as well, since cleavage of both strands is modeled as concurrent, and dissociation of cleaved DNA leads to equal concentrations of top and bot strands. Since the baseline and scaling factors are different for the Flo and Rox quantification in the urea-PAGE gel, the reactions with each strand were quantitated and subsequently fit separately for each in each reaction.

Table S15. Additional equations added to *"Filament Assembly EO"* to allow up to 9mers

Reaction Step	Forward Rate Constant	Reverse Rate Constant
Self-assembly of SgrAI/DNA Complexes (SgrAI/A-DNA complex is denoted as A, SgrAI/R-DNA complex is denoted as R)		
Self-associations where SgrAI/A-DNA (i.e. A) binds to another SgrAI/A-DNA (i.e. A)		
ARAA+A ⇌ ARAAA	k_4	k_{-4}
A+ARAA ⇌ AARAA	k_4	k_{-4}
ARAA+A ⇌ ARAAA	k_4	k_{-4}
A+ARAA ⇌ AARAA	k_4	k_{-4}
AARA+A ⇌ AARAA	k_4	k_{-4}
A+AARA ⇌ AAARA	k_4	k_{-4}
A+AAAR ⇌ AAAAR	k_4	k_{-4}
RAAA+A ⇌ RAAAA	k_4	k_{-4}
ARAAA+A ⇌ ARAAAA	k_4	k_{-4}
A+ARAAA ⇌ AARAAA	k_4	k_{-4}
AARAA+A ⇌ AARAAA	k_4	k_{-4}
A+AARAA ⇌ AAARAA	k_4	k_{-4}
AAARA+A ⇌ AAARAA	k_4	k_{-4}
A+AAARA ⇌ AAAARA	k_4	k_{-4}
RAAAA+A ⇌ RAAAAA	k_4	k_{-4}
ARAAAA+A ⇌ ARAAAAA	k_4	k_{-4}

A+ARAAAA ⇌ AARAAAA	k_4	k_{-4}
AARAAA+A ⇌ AARAAAA	k_4	k_{-4}
A+AARAAA ⇌ AAARAAA	k_4	k_{-4}
AAARAA+A ⇌ AAARAAA	k_4	k_{-4}
A+AAARAA ⇌ AAAARAA	k_4	k_{-4}
AAAARA+A ⇌ AAAARAA	k_4	k_{-4}
A+AAAARA ⇌ AAAAARA	k_4	k_{-4}
RAAAAA+A ⇌ RAAAAAA	k_4	k_{-4}
ARAAAA+A ⇌ ARAAAAA	k_4	k_{-4}
A+ARAAAA ⇌ AARAAAA	k_4	k_{-4}
ARAAAAA+A ⇌ ARAAAAAA	k_4	k_{-4}
A+ARAAAAA ⇌ AARAAAAA	k_4	k_{-4}
AARAAAA+A ⇌ AARAAAAA	k_4	k_{-4}
A+ AARAAAA ⇌ AAARAAAA	k_4	k_{-4}
AARAAAA+A ⇌ AARAAAAA	k_4	k_{-4}
A+AARAAAA ⇌ AAARAAAA	k_4	k_{-4}
AAARAAA+A ⇌ AAARAAAA	k_4	k_{-4}
A+AAARAAA ⇌ AAAARAAA	k_4	k_{-4}
AAAARAA+A ⇌ AAAARAAA	k_4	k_{-4}
A+ AAAARAA ⇌ AAAAARAA	k_4	k_{-4}
AAAAARA+A ⇌ AAAAARAA	k_4	k_{-4}
A+ AAAAARA ⇌ AAAAAARA	k_4	k_{-4}
A+AAAAARAA ⇌ AAAAAARAA	k_4	k_{-4}
AAAAARAA+A ⇌ AAAAARAAA	k_4	k_{-4}
*Associations where SgrAI/**R-DNA** (i.e. R) binds to a SgrAI/**A-DNA** (i.e. A)*		
A+RAAA ⇌ ARAAA	k_5	k_{-5}
A+RAAA ⇌ ARAAA	k_5	k_{-5}
A+RAAAA ⇌ ARAAAA	k_5	k_{-5}
AAAR+A ⇌ AAARA	k_5	k_{-5}
AAAAR+A ⇌ AAAARA	k_5	k_{-5}
A+RAAAAA ⇌ ARAAAAA	k_5	k_{-5}

Table S16. Additional terms to add to the *"Filament Assembly 5EO"* model to predict FRET signal for ROO filaments containing up to 9 SgrAI/DNA complexes.

Equation
(2a+b+c)[ARAAA]+(2a+2b)[AARAA]+(2a+2b+c)[AAARA]+(a+b+c)[AAAAR]+(a+b+c)[RAAAA]+(2a+b+c)[ARAAAA]+(2a+2b+c)[AARAAA]+(2a+2b+c)[AAARAA]+(2a+b+c)[AAAARA]+(a+b+c)[RAAAAAA]+(2a+b+c)[ARAAAAA]+(2a+2b+c)[AARAAAA]+(2a+2b+2c)[AAARAAAA]+(2a+2b+c)[AAAARAA]+(2a+b+c)[AAAAARA]+(2a+b+c)[ARAAAAAA]+(2a+2b+c)[AARAAAAA]+(2a+2b+2c)[AAARAAAA]+(2a+2b+2c)[AAAARAAA]+(2a+2b+c)[AAAAARAA]+(2a+b+c)[AAAAAARA]+(2a+2b+c)[AAAAAARAA]+(2a+2b+2c)[AAAAARAAA]

REFERENCES

1. Park, C. K., Stiteler, A. P., Shah, S., Ghare, M. I., Bitinaite, J., and Horton, N. C. (2010) Activation of DNA cleavage by oligomerization of DNA-bound SgrAI. *Biochemistry* **49**, 8818-8830
2. Park, C. K., Sanchez, J. L., Barahona, C. J., Basantes, L. E., Sanchez, J., Hernandez, C., and Horton, N. C. (2018) The Run-On Oligomer Filament Enzyme Mechanism of SgrAI. Part 1: Assembly Kinetics of the Run-On Oligomer

Filament. *Submitted for publication*
3. Johnson, K. A., Simpson, Z.B., Blom, T. (2009) Global Kinetic Explorer: A new computer program for dynamic simulation and fitting of kinetic data. *Analytical Biochemistry* **387**, 20-29